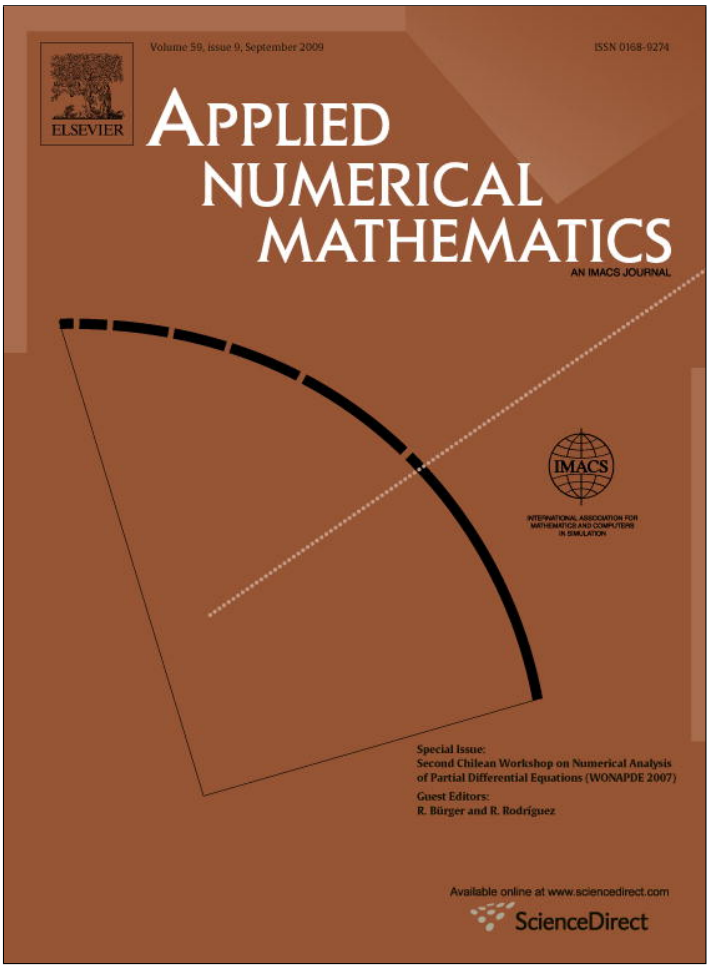

Applied Numerical Mathematics 59 (2009) 2082–2104

Contents lists available at ScienceDirect

Applied Numerical Mathematics

www.elsevier.com/locate/apnum

Numerical simulation of a thermo-electromagneto-hydrodynamic problem in an induction heating furnace ☆

A. Bermúdez *, D. Gómez, M.C. Muñiz, P. Salgado, R. Vázquez

Departamento de Matemática Aplicada, Universidade de Santiago de Compostela, 15782 Santiago de Compostela, Spain

ARTICLE INFO

Article history:
Available online 14 December 2008

Keywords:
Numerical methods
Thermo-magneto-hydrodynamic
Induction furnaces
Change of phase
Coupled problems

ABSTRACT

This paper deals with mathematical modelling and numerical simulation of induction heating furnaces with axisymmetric geometries. The mathematical model consists of a coupled thermo-electromagneto-hydrodynamic problem with phase change. For the numerical solution, we propose finite element methods combined with boundary element methods (BEM/FEM) for the electromagnetic model, and with the method of characteristics for the flow equations. Moreover, an iterative fixed point-like algorithm is established for the whole coupling. Some numerical results for an industrial furnace are shown.

1. Introduction

In the past years, induction heating techniques have been widely applied in the metallurgical and semiconductor industry, in processes such as metal smelting [14,16,27], metal hardening [13,28] or crystal growth [15,22]. An induction heating system basically consists of one or several inductors supplied with an alternating electrical current and a metallic workpiece to be heated. Based on this idea, different kinds of induction furnaces can be designed depending on the application. Thus, in the past years, with the growth of the photovoltaic industry and the increasing request for high purity silicon, greater efforts have been made to design operative induction furnaces devoted to the silicon purification [7–9].

This work concerns an induction furnace like the one represented in Fig. 1. It consists of a cylindrical vessel (usually called the crucible) made from a material such as graphite, surrounded by an inductor coil made of a very conductive material (copper, for instance), and containing the material to be heated (silicon, in our case) in its interior. The main idea of the process is quite simple: the coil is supplied with alternating current that produces a rapidly oscillating magnetic field which, in its turn, induces eddy currents. These eddy currents, due to the Joule effect, cause heat losses and consequently the electrically conducting materials of the workpiece are heated.

The purification process is based on the fact that most of the impurities tend to remain in the molten region rather than re-solidify. Controlling this melting-solidifying process enable us to localize most of the impurities near to the liquid surface. The inductive system can indeed be designed to maintain the silicon in a liquid state, control the shape of its free surface and provide a strong electromagnetic stirring, ensuring a rapid transfer of pollutants from the liquid bulk to its surface. An important advantage of induction heating is the efficiency in stirring the liquid metal due to the Lorentz forces generated by the induced fields. This stirring also improves the melting since the moving fluid transfers heat from the crucible wall to

☆ Supported by Xunta de Galicia under research project PGIDIT06PXIB207052PR and by Ministerio de Educación y Ciencia (Spain) under research project Consolider MATHEMATICA CSD2006-00032. The last author has been supported by a predoctoral grant FPI from the Spanish Ministry of Education and Science, cofinanced by the European Social Fund.

* Corresponding author.
E-mail address: alfredo.bermudez@usc.es (A. Bermúdez).

0168-9274/$30.00
doi:10.1016/j.apnum.2008.12.005

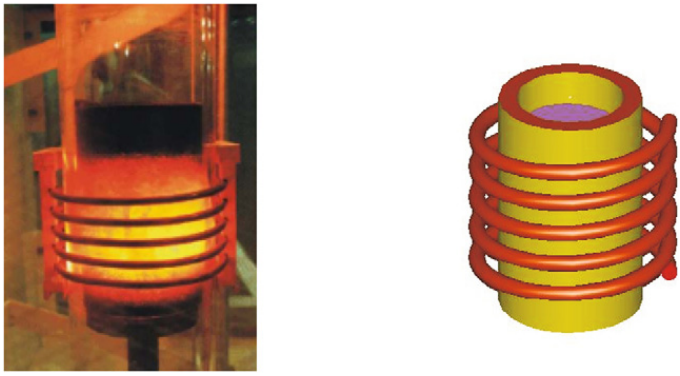

Fig. 1. Induction furnace (left) and sketch of the geometry (right).

the solid. The numerical simulation can be used to control the global design of the induction system, analyzing, for instance, the effect of the power and the frequency on the process.

The overall process is rather complex, involving thermal, electromagnetic and hydrodynamic phenomena. From the mathematical point of view, and in order to perform a numerical simulation of the furnace, the physical process is expressed as a coupled non-linear system of partial differential equations arising from the thermo-electromagneto-hydrodynamic problem. In the past years several papers have been published dealing with the thermo-electromagnetic problem [5,7,8,14,16,22], with the electromagneto-hydrodynamic problem [18,24] or with the thermo-electromagneto-hydrodynamic problem [17,21], but not fully coupled because materials properties are supposed to be independent of temperature.

The electromagnetic model presented in this paper is based on the time-harmonic eddy current problem and has been numerically solved by using a finite element method in [7] and a hybrid BEM/FEM in [8]. In both cases, the formulation is based on a particular magnetic vector potential and the current intensities flowing through the inductor coil are imposed in a weak form. In the present work, we complete the electromagnetic model from a mathematical point of view; we focus mainly on the technique to impose the current intensities in a weak form and prove that the corresponding mixed problem is well posed. For the numerical solution, we propose the BEM/FEM already used in [8]. Furthermore, we improve the thermal model presented in [7,8] by including convective heat transfer which leads us to introduce the numerical solution of a hydrodynamic problem. The numerical results will illustrate the importance of considering the convective effects when computing the temperature field. On the other hand, the computation of the velocity field in the molten silicon, allows us to control the movement of the impurities towards the surface.

The outline of this paper will be as follows. In Section 2 we will state the overall problem and the electromagnetic submodel. In Section 3 the thermal submodel will be introduced using the enthalpy in order to take into account the phase change. In Section 4 we will present the hydrodynamic model by using the incompressible Reynolds-averaged Navier–Stokes equations to handle the effects of turbulence. In Section 5 we will introduce a time-discretization of the coupled problem and propose an iterative algorithm for its solution. Finally, in Section 6 we will present some numerical results, the first concerning an academic problem, and the second presenting a numerical simulation of an industrial furnace for silicon purification.

2. Statement of the problem

An induction furnace consisting of a helical coil surrounding a crucible as the one sketched in Fig. 1 is used as the basis for the problem. The electrically conducting crucible contains the material to be heated and it is surrounded by a refractory material to avoid heat losses. An alternating low frequency current passing through the coil produces an oscillating magnetic field which generates eddy currents in the workpiece. These currents, due to the Joule effect, produce heat in the conducting crucible in such a way that the metal is also heated until it melts.

In order to state the problem in an axisymmetric setting, the induction coil has to be replaced by m rings having toroidal geometry. Let Ω_0 be the radial section of the workpiece and $\Omega_1, \Omega_2, \ldots, \Omega_m$ be the radial sections of the turns of the coil. Moreover, we denote by Ω the radial section of the set of conductors, i.e., inductors and workpiece, given by (see Fig. 3),

$$\Omega = \bigcup_{k=0}^{m} \Omega_k$$

and $\Omega^c = \mathbb{R}^2 \setminus \bar{\Omega}$. Let $\Delta \subset \mathbb{R}^3$ be the bounded open set generated by the rotation about the z-axis of Ω and Δ^c the complementary set of $\bar{\Delta}$ in $\mathbb{R}^3$. Notice that Δ^c is an unbounded set corresponding to the air surrounding the whole device. Analogously, we denote by Δ_k, $k = 0, \ldots, m$ the subset of $\mathbb{R}^3$ generated by the rotation of Ω_k, $k = 0, \ldots, m$, respectively, around the z-axis (see Fig. 2). In particular, Ω_0 is supposed to be simply connected.

We denote by Σ the boundary of Δ and by Γ its intersection with the half-plane $\{(r, z) \in \mathbb{R}^2; r > 0\}$. Moreover, we assume that the boundary of Ω is the union of Γ and Γ_s, the latter being a subset of the symmetry axis (see Fig. 3).

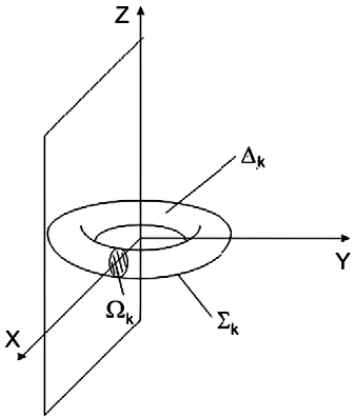

Fig. 2. Sketch of a toroidal turn Δ_k.

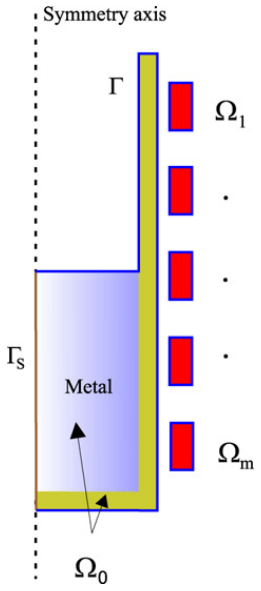

Fig. 3. Radial section of inductors and workpiece.

2.1. The electromagnetic model

In this section we present the electromagnetic model and perform the mathematical analysis of the resulting weak formulation. The analysis is developed in the framework of the 3D-problem in order to cover more general applications, which do not present cylindrical symmetry. In particular, Δ is not necessarily axisymmetric, but Δ_0 must be simply connected and each Δ_k, $k = 1, \ldots, m$, must be like a torus, in the sense that it is enough one cutting surface Ω_k for the set $\Delta_k \setminus \Omega_k$ being simply–connected.

Since we are considering alternating currents, we assume that all of the fields have the form:

$$\mathcal{F}(\mathbf{x}, t) = \mathrm{Re}\left[e^{i\omega t}\mathbf{F}(\mathbf{x})\right], \tag{1}$$

where t is time, $\mathbf{x} \in \mathbb{R}^3$ is the space position, ω is the angular frequency, i the imaginary unit and $\mathbf{F}(\mathbf{x})$ is the complex amplitude of the field. Moreover, since the induction furnace we are interested in works in a low-frequency regime, then Maxwell's equations can be reduced to the so-called *eddy current* model (see [11] for a discussion of parameter ranges in which the model is valid):

$$\mathbf{curl}\,\mathbf{H} = \mathbf{J} \quad \text{in } \mathbb{R}^3, \tag{2}$$

$$i\omega\mathbf{B} + \mathbf{curl}\,\mathbf{E} = \mathbf{0} \quad \text{in } \mathbb{R}^3, \tag{3}$$

$$\mathrm{div}\,\mathbf{B} = 0 \quad \text{in } \mathbb{R}^3, \tag{4}$$

where **H**, **J**, **B** and **E** are the complex amplitudes associated with the magnetic field, the current density, the magnetic induction and the electric field.

The system (2)–(4) needs to be completed with the constitutive relations

$$\mathbf{B} = \mu\mathbf{H} \quad \text{in } \mathbb{R}^3, \tag{5}$$

$$\mathbf{J} = \begin{cases} \sigma\mathbf{E} & \text{in } \Delta, \\ \mathbf{0} & \text{in } \Delta^c, \end{cases} \tag{6}$$

where μ is the magnetic permeability and σ is the electric conductivity. Both are supposed to be bounded from below by a positive constant.

Moreover, we have the following behavior at infinity

$$\mathbf{E}(\mathbf{x}) = O\big(|\mathbf{x}|^{-1}\big), \quad \text{uniformly for } |\mathbf{x}| \to \infty, \tag{7}$$

$$\mathbf{H}(\mathbf{x}) = O\big(|\mathbf{x}|^{-1}\big), \quad \text{uniformly for } |\mathbf{x}| \to \infty. \tag{8}$$

The model (2)–(8) must be completed with some *source data* related to the energizing device, which has been removed from the system. In particular, we would like to impose the current intensities $\mathbf{I} = (I_1, \ldots, I_m)$ crossing each transversal section of the inductor, i.e.,

$$\int_{\Omega_k} \mathbf{J}\cdot\boldsymbol{\nu} = I_k, \quad k=1,\dots,m, \tag{9}$$

where $\boldsymbol{\nu}$ denotes a unit normal vector to the sections Ω_k.

Remark 2.1. In order to add the constraints given in (9) to the model, we will have to relax some of Eqs. (2)–(8). This need is due to the fact that problem (2)–(9) does not admit solution unless all the prescribed intensities I_k are null. Indeed, multiplying the conjugate of (3) and (2) by $\mathbf{H}$ and $\bar{\mathbf{E}}$, respectively, integrating over $\mathbb{R}^3$ and using (7), (8) it is straightforward to conclude that fields $\mathbf{B}$ and $\mathbf{E}$ vanish in $\mathbb{R}^3$, and then, $\mathbf{J}$ and the vector $\mathbf{I}$ also vanish.

To overcome this difficulty, throughout this paper, we are going to relax Eq. (3) and consider it in conductor and dielectric separately,

$$\mathrm{i}\omega\mathbf{B} + \mathbf{curl}\,\mathbf{E} = \mathbf{0} \quad \text{in } \Delta, \tag{10}$$

$$\mathrm{i}\omega\mathbf{B} + \mathbf{curl}\,\mathbf{E} = \mathbf{0} \quad \text{in } \Delta^{\mathrm{c}}. \tag{11}$$

In Remark 2.2, we will detail another alternative to impose the current intensities, based on the modification of the Ohm's law in Δ. This option has been proposed, for instance in [2], in the context of bounded domains.

In order to solve the problem, we start by introducing a magnetic vector potential and a suitable scalar potential.

Firstly, Eq. (4) allows us to affirm that there exists a magnetic vector potential $\mathbf{A}$, defined in $\mathbb{R}^3$, such that,

$$\mathbf{B} = \mathbf{curl}\,\mathbf{A}, \tag{12}$$

and from Eq. (10), we obtain

$$\mathrm{i}\omega\,\mathbf{curl}\,\mathbf{A} + \mathbf{curl}\,\mathbf{E} = \mathbf{0} \quad \text{in } \Delta.$$

Now, taking into account the form of the kernel of the **curl** operator in each connected component of the conductor, we can say that (see, for instance [3])

$$\mathrm{i}\omega\mathbf{A} + \mathbf{E} = -\mathbf{v} \quad \text{in } \Delta, \tag{13}$$

where

$$\mathbf{v} = \widetilde{\mathbf{grad}}\,\tilde{U},$$

with $\tilde{U}$ being a scalar potential having a constant jump through each Ω_k, for $k=1,\dots,m$. Here and in the rest of the paper $\widetilde{\mathbf{grad}}$ denotes the gradient operator in the space $\mathrm{H}^1(\Delta\setminus\bigcup_{k=1}^m\Omega_k)$.

As we will show below, this representation allows us to impose the sources inside the closed circuits Δ_k (see also Section 5.2 of [20]). However, in general we will not be able to extend $\mathbf{v}$ to Δ^{c} having continuous tangential trace on Σ. We will return later to this question.

For $k=1,\dots,m$, let us denote by η_k the solution in $\mathrm{H}^1(\Delta_k\setminus\Omega_k)$, unique up to a constant, of the following weak problem:

$$\int_{\Delta_k\setminus\Omega_k} \sigma\,\widetilde{\mathbf{grad}}\,\eta_k\cdot\mathbf{grad}\,\xi = 0 \quad \forall\xi\in\mathrm{H}^1(\Delta_k), \tag{14}$$

$$[\eta_k]_{\Omega_k} = 1, \tag{15}$$

where $[\eta_k]_{\Omega_k}$ denotes the jump of η_k through Ω_k along $\boldsymbol{\nu}$.

By using functions η_k, $k=1,\dots,m$, the scalar potential $\tilde{U}$ can be written as (see again [3]),

$$\tilde{U} = \Phi + \sum_{k=1}^m V_k\eta_k, \tag{16}$$

with $\Phi\in\mathrm{H}^1(\Delta)$ and $V_k, k=1,\dots,m$, some complex numbers. From the definition of η_k we deduce that V_k is the constant jump of $\tilde{U}$ through each surface Ω_k, $k=1,\dots,m$. From a physical point of view, these complex numbers V_k, can be interpreted as voltage drops (see, for instance, [20]).

Then, taking into account that $\mathbf{H} = \mu^{-1}\,\mathbf{curl}\,\mathbf{A}$ and Eq. (2) we obtain

$$\mathrm{i}\omega\sigma\mathbf{A} + \mathbf{curl}\left(\frac{1}{\mu}\,\mathbf{curl}\,\mathbf{A}\right) = -\sigma\mathbf{v} = -\sigma\left(\mathbf{grad}\,\Phi + \sum_{k=1}^m V_k\,\widetilde{\mathbf{grad}}\,\eta_k\right). \tag{17}$$

Notice, however, that the vector potential $\mathbf{A}$ is not unique because it can be altered by any gradient. Thus, in order to get uniqueness we need to impose some *gauge conditions*.

Firstly, we set $\operatorname{div}(\sigma\mathbf{A}) = 0$ in the conductor Δ and the boundary condition $\sigma\mathbf{A}\cdot\mathbf{n} = 0$ on Σ, where $\mathbf{n}$ is a unit normal vector to Σ outward from Δ. Moreover, by using (17) and the fact that

$$\mathbf{curl}\left(\frac{1}{\mu}\,\mathbf{curl}\,\mathbf{A}\right)\cdot\mathbf{n} = \mathbf{curl}\,\mathbf{H}\cdot\mathbf{n} = \mathbf{J}\cdot\mathbf{n} = 0 \quad \text{on } \Sigma, \tag{18}$$

the two gauge conditions above lead to $\operatorname{div}(\sigma\mathbf{v}) = 0$ in Δ and $\sigma\mathbf{v}\cdot\mathbf{n} = 0$ on Σ, which can be written in weak form as

$$\int_{\Delta} \sigma\mathbf{v}\cdot\mathbf{grad}\,\xi = 0 \quad \forall\xi \in \mathrm{H}^1(\Delta). \tag{19}$$

By subtracting Eqs. (14) multiplied by V_k, for $k = 1,\dots,m$, from (19), we get

$$\int_{\Delta} \sigma\,\mathbf{grad}\,\Phi\cdot\mathbf{grad}\,\xi = 0 \quad \forall\xi \in \mathrm{H}^1(\Delta), \tag{20}$$

which implies $\mathbf{grad}\,\Phi = \mathbf{0}$ in Δ and hence

$$\mathbf{v} = \sum_{k=1}^{m} V_k\,\widetilde{\mathbf{grad}}\,\eta_k. \tag{21}$$

Secondly, following [4], in the air Δ^{c} we impose the gauge conditions

$$\operatorname{div}\mathbf{A} = 0 \quad \text{in } \Delta^{\mathrm{c}} \quad \text{and} \quad \int_{\Sigma_j} \mathbf{A}\cdot\mathbf{n} = 0, \quad j = 1,\dots,N_c, \tag{22}$$

where $\{\Sigma_j\}_{j=1}^{N_c}$ denotes the connected components of Σ. We notice that $\mathbf{A} \in \mathrm{H}(\operatorname{div},\Delta^{\mathrm{c}})$, but we are not going to assume that $\mathbf{A} \in \mathrm{H}(\operatorname{div},\mathbb{R}^3)$ so the normal trace $\mathbf{A}\cdot\mathbf{n}$ on Σ may be discontinuous and hence the integral conditions in (22) are not redundant.

Next, we obtain a weak formulation of Eqs. (17) and (22). We will come back later to conditions (9).

2.2. Weak formulation

In order to propose a weak formulation of the previous problem we introduce some functional spaces and sets. Let $\boldsymbol{\mathcal{X}}$ be the Beppo–Levi space (see [25], Section 2.5.4)

$$\boldsymbol{\mathcal{X}} = \left\{\mathbf{G}:\ \frac{\mathbf{G}(\mathbf{x})}{\sqrt{1+|\mathbf{x}|^2}} \in \mathbf{L}^2\big(\mathbb{R}^3\big),\ \mathbf{curl}\,\mathbf{G} \in \mathbf{L}^2\big(\mathbb{R}^3\big)\right\},$$

and its subset

$$\boldsymbol{\mathcal{Y}} = \left\{\mathbf{G} \in \boldsymbol{\mathcal{X}} : \operatorname{div}\mathbf{G} = 0 \quad \text{in } \Delta^{\mathrm{c}},\ \int_{\Sigma_j} \mathbf{G}\cdot\mathbf{n} = 0,\ \ j = 1,\dots,N_c\right\}.$$

On the other hand, we assume, in a first step, that the complex numbers V_k are given, for $k = 1,\dots,m$ and try to find the vector potential $\mathbf{A}$. After that, we will show how to solve the problem by giving the intensity vector $\mathbf{I} = (I_1,\dots,I_m)$ as data.

Multiplying Eq. (17) by the complex conjugate of a test function $\mathbf{G}$, denoted by $\bar{\mathbf{G}}$, integrating in $\mathbb{R}^3$ and using a Green's formula we can easily obtain the following weak formulation:

Problem PV. Given $\mathbf{V} = (V_1,\dots,V_m) \in \mathbb{C}^m$, find $\mathbf{A} \in \boldsymbol{\mathcal{Y}}$ such that

$$\mathrm{i}\omega\int_{\mathbb{R}^3} \sigma\mathbf{A}\cdot\bar{\mathbf{G}} + \int_{\mathbb{R}^3} \frac{1}{\mu}\,\mathbf{curl}\,\mathbf{A}\cdot\mathbf{curl}\,\bar{\mathbf{G}} = -\sum_{k=1}^{m} V_k \int_{\Delta_k\setminus\Omega_k} \sigma\,\widetilde{\mathbf{grad}}\,\eta_k\cdot\bar{\mathbf{G}}, \quad \forall\mathbf{G} \in \boldsymbol{\mathcal{Y}}. \tag{23}$$

Remark 2.2. In order to impose the current intensities across the inductors and to avoid relaxing the Faraday's law as we did in previous sections, the authors of [2] propose to modify the Ohm's law as follows

$$\mathbf{J} = \sigma\mathbf{E} - \sigma\sum_{k=1}^{m} V_k\,\widetilde{\mathbf{grad}}\,\eta_k \quad \text{in } \Delta. \tag{24}$$

Notice that, in this way, the current density is divided into two parts: $\sigma\mathbf{E}$ and a source term which is distributed in the coils Δ_k. Then, by using the Faraday's law in $\mathbb{R}^3$, we notice that Eq. (13) reads

$$\mathrm{i}\omega\mathbf{A}+\mathbf{E}=-\,\mathbf{grad}\,\Phi \quad \text{in } \mathbb{R}^3, \tag{25}$$

and arguing as in the rest of Section 2.1, we can arrive at the same weak problem **PV**.

Theorem 2.1. *Problem* **PV** *has a unique solution.*

Proof. Since the function

$$\mathbf{J}_0 := -\sigma \sum_{k=1}^{m} V_k \widetilde{\mathbf{grad}}\,\eta_k$$

belongs to $\mathbf{L}^2(\Delta)$ the result is an immediate consequence of Theorem 2.1 in [19]. □

The next proposition is a straightforward adaptation to unbounded domains of results included in the Section 2 of [1]:

Proposition 2.1. *Let* $\mathbf{A}$ *be the unique solution of problem* **PV**. *Then Eq.* (23) *also holds for any* $\mathbf{G}\in\boldsymbol{\mathcal{X}}$.

Theorem 2.2. *Given* $\mathbf{V}=(V_1,\ldots,V_m)\in\mathbb{C}^m$, *let* $\mathbf{A}$ *be the solution of problem* **PV**. *Let us define* $\mathbf{B}:=\mathbf{curl}\,\mathbf{A}$, $\mathbf{H}:=\frac{1}{\mu}\mathbf{B}$, $\mathbf{E}:=-\mathrm{i}\omega\mathbf{A}-\sum_{k=1}^{m} V_k\widetilde{\mathbf{grad}}\,\eta_k$ *in* Δ, $\mathbf{J}|_{\Delta}:=\sigma\mathbf{E}$ *and* $\mathbf{J}|_{\Delta^{\mathrm{c}}}:=\mathbf{0}$. *Then the following equalities hold true*:

$$\mathbf{curl}\,\mathbf{H}=\mathbf{J} \quad \text{in } \mathbb{R}^3, \tag{26}$$

$$\mathrm{i}\omega\mathbf{B}+\mathbf{curl}\,\mathbf{E}=\mathbf{0} \quad \text{in } \Delta, \tag{27}$$

$$\mathrm{div}\,\mathbf{B}=0 \quad \text{in } \mathbb{R}^3, \tag{28}$$

$$\mathbf{J}\cdot\mathbf{n}=0 \quad \text{on } \Sigma. \tag{29}$$

Proof. We notice that, from the previous proposition we are allowed to take as test function $\mathbf{G}$ in (23) any smooth function with compact support in $\mathbb{R}^3$. By doing so, we obtain,

$$\mathrm{i}\omega\sigma\mathbf{A}+\mathbf{curl}\left(\frac{1}{\mu}\,\mathbf{curl}\,\mathbf{A}\right)+\sigma\sum_{k=1}^{m} V_k\widetilde{\mathbf{grad}}\,\eta_k=\mathbf{0} \quad \text{in } \mathbb{R}^3 \tag{30}$$

in the sense of distributions. Hence, in particular, $\mathbf{curl}(\mu^{-1}\,\mathbf{curl}\,\mathbf{A})$ belongs to $\mathbf{L}^2(\mathbb{R}^3)$. Then, if we define the magnetic induction $\mathbf{B}$ in $\mathbb{R}^3$ as

$$\mathbf{B}:=\mathbf{curl}\,\mathbf{A},$$

the magnetic field as $\mathbf{H}:=\mu^{-1}\mathbf{B}$, the electric field by

$$\mathbf{E}:=-\mathrm{i}\omega\mathbf{A}-\sum_{k=1}^{m} V_k\widetilde{\mathbf{grad}}\,\eta_k \quad \text{in } \Delta, \tag{31}$$

$\mathbf{J}|_{\Delta}:=\sigma\mathbf{E}$ and $\mathbf{J}|_{\Delta^{\mathrm{c}}}:=\mathbf{0}$, we clearly obtain Eqs. (26) and (28) from (30).

Moreover, since $\mathbf{curl}\,\mathbf{H}=\mathbf{J}$ in $\mathbf{L}^2(\mathbb{R}^3)$, then $\mathrm{div}\,\mathbf{J}=0$. Hence the trace $\mathbf{J}\cdot\mathbf{n}$ is well defined on Σ and $\mathbf{J}\cdot\mathbf{n}=0$ there since $\mathbf{J}$ vanishes in Δ^{c}.

Finally, we can take the **curl** operator in (31) to get

$$\mathbf{curl}\,\mathbf{E}=-\mathrm{i}\omega\mathbf{B} \quad \text{in } \Delta,$$

because $\mathbf{curl}\,\widetilde{\mathbf{grad}}\equiv\mathbf{0}$. □

Remark 2.3. If we define a curl-free extension of $\mathbf{v}$ to Δ^{c} and $\mathbf{E}:=-\mathrm{i}\omega\mathbf{A}-\mathbf{v}$, then the Faraday's law also holds in this set. However, one can easily show (see [20]) that there is no such extension belonging to the space $\boldsymbol{\mathcal{X}}$. The conclusion is that one cannot define $\mathbf{E}$ in $\boldsymbol{\mathcal{X}}$ so as to satisfy the eddy current model in the whole space together with the conditions prescribing non-null intensities in the rings Δ_k.

Remark 2.4. Notice that, from the definition of $\mathbf{E}$ and the properties $\operatorname{div}(\sigma\mathbf{E}) = 0$ in Δ (which follows from (26)), and $\sigma\mathbf{E}\cdot\mathbf{n} = 0$ on Σ, we can deduce that the solution $\mathbf{A}$ of problem **PV** also satisfies the imposed gauge conditions in the conductor, i.e.,

$$\operatorname{div}(\sigma\mathbf{A}) = 0 \quad \text{in } \Delta, \tag{32}$$

$$\sigma\mathbf{A}\cdot\mathbf{n} = 0 \quad \text{on } \Sigma. \tag{33}$$

We recall that the gauge conditions in the dielectric are directly imposed in the space $\mathcal{Y}$.

Remark 2.5. Under the modified Ohm's law approach, the electric field $\mathbf{E}$ and the current density $\mathbf{J}$ in Theorem 2.2 have to be redefined by

$$\mathbf{E} = -\mathrm{i}\omega\mathbf{A} \quad \text{in } \mathbb{R}^3, \tag{34}$$

$$\mathbf{J} = \sigma\mathbf{E} - \sigma\sum_{k=1}^{m} V_k\,\widetilde{\mathbf{grad}}\,\eta_k \quad \text{in } \Delta, \tag{35}$$

and (27) holds in $\mathbb{R}^3$.

2.3. Imposing the current intensities in a weak sense

We recall that we are interested in finding a solution of the eddy current problem satisfying the intensities conditions (9). To attain this goal, we start by writing these constraints in a weak sense.

Firstly, we notice that, since the current density $\mathbf{J} = \sigma\mathbf{E}$ satisfies $\operatorname{div}\mathbf{J} = 0$ in Δ and $\mathbf{J}\cdot\mathbf{n} = 0$ on Σ, we have

$$\int_{\Delta_k\setminus\Omega_k} \mathbf{J}\cdot\widetilde{\mathbf{grad}}\,\eta_k = -\int_{\Delta_k\setminus\Omega_k} \operatorname{div}\mathbf{J}\,\eta_k + \int_{\partial(\Delta_k\setminus\Omega_k)} \mathbf{J}\cdot\mathbf{n}\,\eta_k = \int_{\Omega_k} [\eta_k]\mathbf{J}\cdot\boldsymbol{\nu} = I_k, \tag{36}$$

$k = 1,\dots,m$. Thus, we can impose the current intensities as follows:

$$\sum_{k=1}^{m} \bar{W}_k \int_{\Delta_k\setminus\Omega_k} \sigma\mathbf{E}\cdot\widetilde{\mathbf{grad}}\,\eta_k = \sum_{k=1}^{m} I_k\bar{W}_k, \quad \forall\mathbf{W} = (W_1,\dots,W_m)\in\mathbb{C}^m.$$

Then, taking into account (31), we obtain the following weak form of constraint (9) which is well defined for any vector function $\mathbf{A}\in\mathcal{Y}$:

$$-\sum_{k=1}^{m} \bar{W}_k \int_{\Delta_k\setminus\Omega_k} \mathrm{i}\omega\sigma\,\widetilde{\mathbf{grad}}\,\eta_k\cdot\mathbf{A} - \sum_{k=1}^{m} \bar{W}_k \int_{\Delta_k\setminus\Omega_k} \sigma V_k|\widetilde{\mathbf{grad}}\,\eta_k|^2 = \sum_{k=1}^{m} I_k\bar{W}_k, \quad \forall\mathbf{W}\in\mathbb{C}^m. \tag{37}$$

Therefore, given the vector field $\mathbf{I} = (I_1,\dots,I_m)$, we are led to solve the following mixed problem:

Problem MPI. Given $\mathbf{I} = (I_1,\dots,I_m)\in\mathbb{C}^m$, find $\mathbf{A}\in\mathcal{Y}$ and $\mathbf{V}\in\mathbb{C}^m$, such that

$$\mathrm{i}\omega\int_{\mathbb{R}^3} \sigma\mathbf{A}\cdot\bar{\mathbf{G}} + \int_{\mathbb{R}^3} \frac{1}{\mu}\,\mathbf{curl}\,\mathbf{A}\cdot\mathbf{curl}\,\bar{\mathbf{G}} + \sum_{k=1}^{m} V_k \int_{\Delta_k\setminus\Omega_k} \sigma\,\widetilde{\mathbf{grad}}\,\eta_k\cdot\bar{\mathbf{G}} = 0, \quad \forall\mathbf{G}\in\mathcal{Y},$$

$$\sum_{k=1}^{m} \bar{W}_k \int_{\Delta_k\setminus\Omega_k} \sigma\,\widetilde{\mathbf{grad}}\,\eta_k\cdot\mathbf{A} + \frac{1}{\mathrm{i}\omega}\sum_{k=1}^{m} \bar{W}_k \int_{\Delta_k\setminus\Omega_k} \sigma V_k|\widetilde{\mathbf{grad}}\,\eta_k|^2 = -\frac{1}{\mathrm{i}\omega}\sum_{k=1}^{m} I_k\bar{W}_k, \quad \forall\mathbf{W}\in\mathbb{C}^m.$$

From the solution $(\mathbf{A},\mathbf{V})$, the vector fields $\mathbf{H}$, $\mathbf{E}$ and $\mathbf{B}$ defined as in Theorem 2.2, would be the solution of the full eddy current model (2)–(9), except that the Faraday's law (3) does not hold on the interface separating the conducting and the dielectric domains.

Notice moreover, that the complex vector of potentials, $\mathbf{V}$, can be interpreted as a Lagrange multiplier introduced to impose the current intensities in a weak sense.

Remark 2.6. Considering the modified Ohm's law approach, Eq. (36) also holds for $\mathbf{J} = \sigma\mathbf{E} - \sigma\sum_{k=1}^{m} V_k\,\widetilde{\mathbf{grad}}\,\eta_k$ and taking into account that $\mathbf{E} = -\mathrm{i}\omega\mathbf{A}$, Eq. (37) is easily obtained. Thus, by modifying the Ohm's law, we also obtain the mixed problem **MPI**.

2.4. Analysis of the mixed problem

An important feature of the mixed problem **MPI** is that the second equation allows us to obtain the components of vector **V** in terms of **I** and **A**. Then, by replacing **V** in the first equation we can obtain a weak problem with **A** being the only unknown, which can be analyzed in a classical setting. To attain this goal, we start by introducing some notation.

Firstly, we define the following scalar product in $\mathbf{L}^2(\Delta_k)$:

$$(\mathbf{F},\mathbf{G})_{\Delta_k,2,\sigma}=\int\limits_{\Delta_k\setminus\Omega_k}\sigma\,\mathbf{F}\cdot\bar{\mathbf{G}},$$

and denote by $\|\cdot\|_{\Delta_k,2,\sigma}$ the corresponding induced norm.

On the other hand, the space of so-called *Neumann harmonic fields* in Δ (see [3]) is defined by

$$\mathcal{C}(\Delta):=\big\{\mathbf{G}\in\mathbf{L}^2(\Delta):\ \mathbf{curl}\,\mathbf{G}=\mathbf{0},\,\mathrm{div}(\sigma\mathbf{G})=0\ \text{in}\ \Delta\ \text{and}\ \sigma\mathbf{G}\cdot\mathbf{n}=\mathbf{0}\ \text{on}\ \Sigma\big\}.$$

A basis of this space is given by the set of orthogonal functions $\{\widetilde{\mathbf{grad}}\,\eta_k,\ k=1,\dots,m\}$ introduced above. In particular, we consider the corresponding orthonormal basis $\{\mathbf{a}_k,\ k=1,\dots,m\}$, given by

$$\mathbf{a}_k=\frac{\widetilde{\mathbf{grad}}\,\eta_k}{\|\widetilde{\mathbf{grad}}\,\eta_k\|_{\Delta_k,2,\sigma}}.$$

Given a vector field $\mathbf{F}\in\mathbf{L}^2(\Delta)$, let us denote by $\mathcal{P}(\mathbf{F})$ its projection on $\mathcal{C}(\Delta)$ defined by

$$\mathcal{P}(\mathbf{F})=\sum_{k=1}^{m}(\mathbf{F},\mathbf{a}_k)_{\Delta_k,2,\sigma}\,\mathbf{a}_k.$$

By using this notation, from the second equation of the mixed problem **MPI**, the components of **V** can be written as:

$$V_k=\frac{-I_k}{\|\widetilde{\mathbf{grad}}\,\eta_k\|^2_{\Delta_k,2,\sigma}}-\mathrm{i}\omega\frac{(\mathbf{A},\mathbf{a}_k)_{\Delta_k,2,\sigma}}{\|\widetilde{\mathbf{grad}}\,\eta_k\|_{\Delta_k,2,\sigma}},\quad k=1,\dots,m. \tag{38}$$

By replacing this expression in the first equation of the mixed problem and taking into account that $\sigma=0$ in Δ^{c}, we have:

$$\mathrm{i}\omega\int\limits_{\Delta}\sigma\mathbf{A}\cdot\bar{\mathbf{G}}+\int\limits_{\mathbb{R}^3}\frac{1}{\mu}\,\mathbf{curl}\,\mathbf{A}\cdot\mathbf{curl}\,\bar{\mathbf{G}}-\mathrm{i}\omega\sum_{k=1}^{m}(\mathbf{A},\mathbf{a}_k)_{\Delta_k,2,\sigma}\int\limits_{\Delta_k\setminus\Omega_k}\sigma\,\mathbf{a}_k\cdot\bar{\mathbf{G}}=\sum_{k=1}^{m}\frac{I_k}{\|\widetilde{\mathbf{grad}}\,\eta_k\|_{\Delta_k,2,\sigma}}\int\limits_{\Delta_k\setminus\Omega_k}\sigma\,\mathbf{a}_k\cdot\bar{\mathbf{G}},\quad\forall\mathbf{G}\in\mathcal{Y}.$$

Thus, the mixed problem **MPI** is equivalent to the following one:

Problem PI. Given $\mathbf{I}=(I_1,\dots,I_m)\in\mathbb{C}^m$, find $\mathbf{A}\in\mathcal{Y}$ satisfying

$$\mathrm{i}\omega\int\limits_{\Delta_0}\sigma\mathbf{A}\cdot\bar{\mathbf{G}}+\int\limits_{\mathbb{R}^3}\frac{1}{\mu}\,\mathbf{curl}\,\mathbf{A}\cdot\mathbf{curl}\,\bar{\mathbf{G}}+\mathrm{i}\omega\sum_{k=1}^{m}\int\limits_{\Delta_k\setminus\Omega_k}\sigma\big(\mathbf{A}-\mathcal{P}(\mathbf{A})\big)\cdot\bar{\mathbf{G}}=\sum_{k=1}^{m}\frac{I_k}{\|\widetilde{\mathbf{grad}}\,\eta_k\|_{\Delta_k,2,\sigma}}\int\limits_{\Delta_k\setminus\Omega_k}\sigma\,\mathbf{a}_k\cdot\bar{\mathbf{G}},\quad\forall\mathbf{G}\in\mathcal{Y}. \tag{39}$$

Theorem 2.3. *Problem* **PI** *has a unique solution.*

Proof. We follow the technique used in Theorem 2.1 of [19] (see also [4]) and some of the results proved in that paper. We introduce the sesquilinear form

$$a(\mathbf{A},\mathbf{G})=\mathrm{i}\omega\sum_{k=0}^{m}\int\limits_{\Delta_k\setminus\Omega_k}\sigma\big(\mathbf{A}-\mathcal{P}(\mathbf{A})\big)\cdot\bar{\mathbf{G}}+\int\limits_{\mathbb{R}^3}\frac{1}{\mu}\,\mathbf{curl}\,\mathbf{A}\cdot\mathbf{curl}\,\bar{\mathbf{G}},$$

taking into account that $\mathcal{P}(\mathbf{A})=\mathbf{0}$ in Δ_0. Using the fact that $(\mathbf{A}-\mathcal{P}(\mathbf{A}),\mathcal{P}(\mathbf{G}))_{\Delta,2,\sigma}=0$ for all $\mathbf{G}\in\mathcal{Y}$ and the estimate concerning the dielectric domain obtained in Theorem 2.1 of [19], we have

$$\big|a(\mathbf{A},\mathbf{A})\big|+\frac{\omega}{\sqrt{2}}\big\|\mathcal{P}(\mathbf{A})\big\|^2_{\Delta,2,\sigma}\geqslant C\left(\|\mathbf{A}\|^2_{\Delta,2,\sigma}+\|\,\mathbf{curl}\,\mathbf{A}\|^2_{\mathbf{L}^2(\mathbb{R}^3)}+\left\|\frac{(\mathbf{A}+\mathbf{w})(\mathbf{x})}{\sqrt{1+|\mathbf{x}|^2}}\right\|^2_{\mathbf{L}^2(\Delta^{\mathrm{c}})}\right) \tag{40}$$

where **w** belongs to a finite dimensional space of harmonic fields in the dielectric domain Δ^{c}.

Taking into account that $\mathcal{P}(\mathbf{A})$ and **w** belong to finite dimensional spaces, we deduce that $a(\cdot,\cdot)$ is $\mathcal{Y}$-coercive, i.e., $\mathcal{Y}$-elliptic modulo a compact perturbation (see again [19]). Then, existence of solution of the weak problem follows from uniqueness.

In order to prove the uniqueness we are going to see that if $\mathbf{I}=\mathbf{0}$, then the solution of problem **PI** is $\mathbf{A}=\mathbf{0}$. Indeed, if $\mathbf{I}=\mathbf{0}$, by taking $\mathbf{G}=\mathbf{A}$ in (39) we deduce that $\mathbf{curl}\,\mathbf{A}=\mathbf{0}$ in $\mathbb{R}^3$ and $\mathbf{A}|_{\Delta}=\mathcal{P}(\mathbf{A})$, and hence $\mathbf{A}\in\mathcal{C}(\Delta)$. Then,

$$\mathbf{A}=-\mathbf{grad}\,\phi$$

with $\phi\in \mathrm{W}^1(\mathbb{R}^3):=\{\psi\colon\ \frac{\psi}{\sqrt{1+|\boldsymbol{x}|^2}}\in \mathrm{L}^2(\mathbb{R}^3),\mathbf{grad}\,\psi\in\mathbf{L}^2(\mathbb{R}^3)\}$ and in particular,

$$\mathbf{A}|_{\Delta}=-\mathbf{grad}\,\phi,\quad \text{with } \phi\in \mathrm{H}^1(\Delta).$$

But then $\mathbf{A}|_{\Delta}=\mathbf{0}$, because $\mathbf{A}$ belongs to $\mathcal{C}(\Delta)$, which is orthogonal to the gradients of functions in $\mathrm{H}^1(\Delta)$.

Moreover, since $\mathbf{A}\in\mathcal{Y}$, it must satisfy, in the dielectric,

$$\mathbf{curl}\,\mathbf{A}=\mathbf{0}\quad \text{in } \Delta^{\mathrm{c}}, \tag{41}$$

$$\operatorname{div}\mathbf{A}=0\quad \text{in } \Delta^{\mathrm{c}}, \tag{42}$$

$$\mathbf{A}\times\mathbf{n}=\mathbf{0}\quad \text{on } \Sigma, \tag{43}$$

$$\int_{\Sigma_j}\mathbf{A}\cdot\mathbf{n}=0\quad j=1,\dots,N_c. \tag{44}$$

Thus, $\mathbf{A}$ belongs to the finite dimensional space of harmonic Dirichlet vector fields in the dielectric defined by,

$$\mathcal{D}\big(\Delta^{\mathrm{c}}\big):=\big\{\mathbf{G}\in\mathbf{L}^2\big(\Delta^{\mathrm{c}}\big)\colon\ \mathbf{curl}\,\mathbf{G}=\mathbf{0},\operatorname{div}\mathbf{G}=0 \text{ in } \Delta^{\mathrm{c}} \text{ and } \mathbf{G}\times\mathbf{n}=\mathbf{0} \text{ on } \Sigma\big\}.$$

Lemma 2.1 in [4] allows us to affirm that a vector field $\mathbf{A}$ satisfying (42) and (44) is orthogonal to the space $\mathcal{D}(\Delta^{\mathrm{c}})$ and since $\mathbf{A}\in\mathcal{D}(\Delta^{\mathrm{c}})$, we conclude that $\mathbf{A}|_{\Delta^{\mathrm{c}}}=\mathbf{0}$. □

Remark 2.7. We have used the equivalence between problems **MPI** and **PI** to analyze the mixed problem. However, since the term involving $\mathcal{P}(\mathbf{A})$ in problem **PI** leads to a fully dense matrix, we will discretize problem **MPI** which leads to matrices where only the last m rows and columns will be dense.

*2.5. An axisymmetric BEM/FEM formulation of problem **MPI***

In order to solve the problem **MPI** by using a BEM/FEM technique, we are going to write this problem in another form involving only the values of the magnetic vector potential $\mathbf{A}$ in Δ and on its boundary Σ. To attain this goal we first notice that the field $\frac{1}{\mu}\,\mathbf{curl}\,\mathbf{A}$, which is the intensity of the magnetic field, belongs to $\mathcal{X}$, and then its tangential trace $\frac{1}{\mu}\,\mathbf{curl}\,\mathbf{A}\times\mathbf{n}$ is continuous across Σ. Besides

$$\mathbf{curl}\left(\frac{1}{\mu_0}\,\mathbf{curl}\,\mathbf{A}\right)=\mathbf{curl}\,\mathbf{H}=\mathbf{0}\quad \text{in } \Delta^{\mathrm{c}}, \tag{45}$$

where μ_0 denotes the vacuum magnetic permeability. Then, by using a Green's formula in Δ^{c}, we have,

$$\begin{aligned}\int_{\mathbb{R}^3}\frac{1}{\mu}\,\mathbf{curl}\,\mathbf{A}\cdot\mathbf{curl}\,\bar{\mathbf{G}}&=\int_{\Delta}\frac{1}{\mu}\,\mathbf{curl}\,\mathbf{A}\cdot\mathbf{curl}\,\bar{\mathbf{G}}+\int_{\Delta^{\mathrm{c}}}\frac{1}{\mu_0}\,\mathbf{curl}\,\mathbf{A}\cdot\mathbf{curl}\,\bar{\mathbf{G}}\\&=\int_{\Delta}\frac{1}{\mu}\,\mathbf{curl}\,\mathbf{A}\cdot\mathbf{curl}\,\bar{\mathbf{G}}+\int_{\Delta^{\mathrm{c}}}\mathbf{curl}\left(\frac{1}{\mu_0}\,\mathbf{curl}\,\mathbf{A}\right)\cdot\bar{\mathbf{G}}-\int_{\Sigma}\frac{1}{\mu_0}\,\mathbf{curl}\,\mathbf{A}\times\mathbf{n}\cdot\bar{\mathbf{G}}\\&=\int_{\Delta}\frac{1}{\mu}\,\mathbf{curl}\,\mathbf{A}\cdot\mathbf{curl}\,\bar{\mathbf{G}}-\int_{\Sigma}\frac{1}{\mu_0}\,\mathbf{curl}\,\mathbf{A}\times\mathbf{n}\cdot\bar{\mathbf{G}},\quad \forall\mathbf{G}\in\mathcal{Y}.\end{aligned}$$

Thus, the first equation of problem **MPI** can be formally written as:

$$\mathrm{i}\omega\int_{\Delta}\sigma\,\mathbf{A}\cdot\bar{\mathbf{G}}+\int_{\Delta}\frac{1}{\mu}\,\mathbf{curl}\,\mathbf{A}\cdot\mathbf{curl}\,\bar{\mathbf{G}}-\int_{\Sigma}\frac{1}{\mu_0}\,\mathbf{curl}\,\mathbf{A}\times\mathbf{n}\cdot\bar{\mathbf{G}}+\sum_{k=1}^{m}V_k\int_{\Delta_k\setminus\Omega_k}\sigma\,\widetilde{\mathbf{grad}}\,\eta_k\cdot\bar{\mathbf{G}}=0,\quad \forall\mathbf{G}\in\mathcal{Y}. \tag{46}$$

We notice that the value of $(1/\mu_0)\,\mathbf{curl}\,\mathbf{A}\times\mathbf{n}$ on Σ can be determined by solving an exterior problem in Δ^{c}. We refer the reader to [19] for the analysis of a BEM/FEM eddy current formulation in terms of the electric field involving this boundary term. However, in this paper, we are more interested in the numerical solution of the problem in an axisymmetric domain Δ and therefore, we will consider a cylindrical coordinate system (r,θ,z) with the z-axis coinciding with the symmetry axis of the device. Hereafter we denote by $\mathbf{e}_r$, $\mathbf{e}_\theta$ and $\mathbf{e}_z$ the local unit vectors in the corresponding coordinate directions.

Now, cylindrical symmetry leads us to consider that no field depends on the angular variable θ. We further assume that the current density field has non-zero component only in the tangential direction $\mathbf{e}_\theta$, namely

$$\mathbf{J} = J_\theta(r,z)\mathbf{e}_\theta.$$

We remark that, due to the assumed conditions on $\mathbf{J}$, (3), (6) and (12), only the θ-component of the magnetic vector potential, hereafter denoted by A_θ, does not vanish, i.e.,

$$\mathbf{A} = A_\theta(r,z)\mathbf{e}_\theta. \tag{47}$$

Note that this $\mathbf{A}$ automatically satisfies (22). Moreover, taking into account the expression for **curl** in cylindrical coordinates we have

$$\mathbf{curl}\,\mathbf{A} = -\frac{\partial A_\theta}{\partial z}\mathbf{e}_r + \frac{1}{r}\frac{\partial (rA_\theta)}{\partial r}\mathbf{e}_z. \tag{48}$$

Let $\mathbf{G} = \psi(r,z)\mathbf{e}_\theta$ be a test function and $\mathbf{n} = n_r\mathbf{e}_r + n_z\mathbf{e}_z$. Thus, taking into account the cylindrical symmetry and the fact that

$$\widetilde{\mathbf{grad}}\,\eta_k = \frac{1}{2\pi r}\mathbf{e}_\theta, \quad \text{in } \Delta_k,\ k=1,\dots,m, \tag{49}$$

the axisymmetric version of problem **MPI** writes formally as follows:

Given $\mathbf{I} = (I_1,\dots,I_m) \in \mathbb{C}^m$, *find* A_θ *and* $\mathbf{V} \in \mathbb{C}^m$, *satisfying,*

$$\begin{aligned} &\mathrm{i}\omega \int_\Omega \sigma A_\theta \cdot \bar{\psi} r\,dr\,dz + \int_\Omega \frac{1}{\mu r}\frac{\partial (rA_\theta)}{\partial r}\frac{\partial (r\bar{\psi})}{\partial r}\,dr\,dz + \int_\Omega \frac{1}{\mu}\frac{\partial A_\theta}{\partial z}\frac{\partial \bar{\psi}}{\partial z}\,r\,dr\,dz \\ &\quad - \int_\Gamma \frac{1}{\mu_0}\frac{\partial (rA_\theta)}{\partial \mathbf{n}}\bar{\psi}\,d\gamma + \frac{1}{2\pi}\sum_{k=1}^m V_k \int_{\Omega_k} \sigma\bar{\psi}\,dr\,dz = 0, \end{aligned} \tag{50}$$

$$\frac{1}{2\pi}\sum_{k=1}^m \Big(\int_{\Omega_k} \sigma A_\theta\,dr\,dz\Big)\bar{W}_k + \frac{1}{4\pi^2\mathrm{i}\omega}\sum_{k=1}^m \Big(\int_{\Omega_k}\sigma\frac{V_k}{r}\,dr\,dz\Big)\bar{W}_k = -\frac{1}{2\pi\,\mathrm{i}\omega}\sum_{k=1}^m I_k\bar{W}_k, \tag{51}$$

where $d\gamma$ *denotes the differential line element.*

The term $\int_\Gamma \mu_0^{-1}\,\partial(rA_\theta)/\partial\mathbf{n}\bar{\psi}\,d\gamma$ can be transformed by using the single-double layer potentials; we refer the reader to [8] for the details concerning this transformation and introduce the same notation of that paper,

$$\begin{aligned} &A'_\theta = rA_\theta, \\ &\lambda'(r,z) = \frac{\partial A'_\theta}{\partial r}n_r + \frac{\partial A'_\theta}{\partial z}n_z. \end{aligned}$$

Then we are led to solve the following weak problem:

Problem WEP. Given $\mathbf{I} = (I_1,\dots,I_m) \in \mathbb{C}^m$, find $A'_\theta : \Omega \to \mathbb{C}$, $\mathbf{V} \in \mathbb{C}^m$ and $\lambda' : \Gamma \to \mathbb{C}$ such that

$$\begin{aligned} &\mathrm{i}\omega\int_\Omega \frac{\sigma}{r}\,A'_\theta\bar{\psi}'\,dr\,dz + \int_\Omega \frac{1}{\mu r}\,\mathbf{grad}\,A'_\theta\cdot\mathbf{grad}\,\bar{\psi}'\,dr\,dz - \int_\Gamma \frac{1}{\mu r}\lambda'\bar{\psi}'\,d\gamma + \sum_{k=1}^m \frac{V_k}{2\pi}\int_{\Omega_k}\frac{\sigma}{r}\bar{\psi}'\,dr\,dz = 0, \quad \forall\,\psi', \\ &\frac{1}{2\pi}\sum_{k=1}^m\Big(\int_{\Omega_k}\frac{\sigma}{r}A'_\theta\,dr\,dz\Big)\bar{W}_k + \frac{1}{4\pi^2\mathrm{i}\omega}\sum_{k=1}^m\Big(\int_{\Omega_k}\sigma\frac{V_k}{r}\,dr\,dz\Big)\bar{W}_k = -\frac{1}{2\pi\,\mathrm{i}\omega}\sum_{k=1}^m I_k\bar{W}_k, \quad \forall\mathbf{W}\in\mathbb{C}^m, \\ &\int_\Gamma \frac{1}{\mu r}\,\bar{\zeta}\,A'_\theta - \int_\Gamma \frac{1}{\mu}(\mathcal{G}_n A'_\theta)\bar{\zeta}(r,z)\,d\gamma + \int_\Gamma \frac{1}{\mu}(\mathcal{G}\lambda')\bar{\zeta}(r,z)\,d\gamma = 0 \quad \forall\zeta, \end{aligned}$$

where $\mathcal{G}$ and $\mathcal{G}_n$ denote the fundamental solution of Laplace's equations and its normal derivative in cylindrical coordinates (see again [8], Eqs. (55), (56)).

3. The thermal model

The electromagnetic model must be coupled with the heat equation to study the thermal effects of the electromagnetic fields in the workpiece. The computational domain for the thermal model is a radial section Ω_0 of the workpiece. Since the metal is introduced in solid state and then melted, we shall use the transient heat transfer equation with change of phase. Furthermore, since the molten metal is subject to electromagnetic and buoyancy forces, we also need to consider convective heat transfer. Let us suppose that we already know the velocity field $\mathbf{u}$ which is null in the solid part of the workpiece, then the equation for energy conservation is

$$\left(\frac{\partial e}{\partial t} + \mathbf{u}\cdot\mathbf{grad}\, e\right) - \mathrm{div}\big(k(\mathbf{x},T)\,\mathbf{grad}\, T\big) = \frac{|\mathbf{J}|^2}{2\sigma} \quad \text{in } \Omega_0, \tag{52}$$

where e is the enthalpy, T is the temperature and k is the thermal conductivity, depending on temperature as well. Hereafter, we also assume that other material properties, such as the electric conductivity σ and the magnetic permeability μ may also depend on temperature. The term $|\mathbf{J}|^2/(2\sigma)$ on the right-hand side of (52) represents the heat released by the electric current due to the Joule effect which is obtained by solving the electromagnetic problem introduced in Section 2. In fact, since the electromagnetic equations are expressed in the frequency domain, the heat source is determined by taking the mean value in a cycle (see [7]).

Note that the terms between parenthesis on the left-hand side of Eq. (52) can be rewritten as the material derivative of enthalpy, which we shall denote by $\dot{e}$. Also, assuming cylindrical symmetry and the fact that T does not depend on the angular coordinate θ, Eq. (52) becomes

$$\dot{e} - \frac{1}{r}\frac{\partial}{\partial r}\left(rk(r,z,T)\frac{\partial T}{\partial r}\right) - \frac{\partial}{\partial z}\left(k(r,z,T)\frac{\partial T}{\partial z}\right) = \frac{|J_\theta|^2}{2\sigma}. \tag{53}$$

Note that, since Δ_0 is a simply connected set, Eq. (13) in cylindrical coordinates reads

$$J_\theta = -\mathrm{i}\omega\sigma A_\theta \quad \text{in } \Omega_0. \tag{54}$$

Eq. (53) must be completed with suitable boundary conditions. We shall denote by $\Gamma_{\mathrm{R}}^{\mathrm{T}}$ the boundary of Ω_0 except for the part corresponding to the symmetry axis which will be denoted by Γ_{S} (see Fig. 4). We consider the radiation–convection condition

$$k(\mathbf{x},T)\frac{\partial T}{\partial \mathbf{n}} = \alpha(T_c - T) + \gamma\left(T_r^4 - T^4\right) \quad \text{on } \Gamma_{\mathrm{R}}^{\mathrm{T}}, \tag{55}$$

α being the coefficient of convective heat transfer, T_c and T_r the external convection and radiation temperatures, respectively and the coefficient γ is the product of emissivity by Stefan–Boltzmann constant. Also, we set

$$k(\mathbf{x},T)\frac{\partial T}{\partial \mathbf{n}} = 0 \quad \text{on } \Gamma_{\mathrm{S}}.$$

4. The hydrodynamic model

As mentioned before, in order to achieve a realistic simulation of the overall process occurring in the furnace, convective heat transfer must be taken into account. The hydrodynamic domain is the molten region of the metal, which varies as the metal melts or solidifies, making our hydrodynamic domain time-dependent.

Let $\Omega_l(t)$ be the radial section of the molten metal, and $\Gamma_{\mathrm{S}}(t)$, $\Gamma_d(t)$ and $\Gamma_n(t)$ the different parts of the boundary at time t (see Fig. 5). We assume that the fluid motion is governed by the incompressible Navier–Stokes equations:

$$\rho(\mathbf{x},T)\left(\frac{\partial \mathbf{u}}{\partial t} + (\mathbf{grad}\,\mathbf{u})\,\mathbf{u}\right) - \mathrm{div}\big(2\eta(\mathbf{x},T)D(\mathbf{u})\big) + \mathbf{grad}\, p = \mathbf{f} \quad \text{in } \Omega_l(t), \tag{56}$$

$$\mathrm{div}\,\mathbf{u} = 0 \quad \text{in } \Omega_l(t), \tag{57}$$

where ρ denotes the density, $\mathbf{u}$ is the velocity field, η is the dynamic viscosity, p is the pressure and $D(\mathbf{u})$ denotes the symmetric part of $\mathbf{grad}\,\mathbf{u}$, namely

$$D(\mathbf{u}) = \frac{\mathbf{grad}\,\mathbf{u} + \mathbf{grad}\,\mathbf{u}^t}{2}.$$

We remark that both density and viscosity are material properties which depend on temperature, i.e., $\rho = \rho(\mathbf{x},T)$ and $\eta = \eta(\mathbf{x},T)$. Moreover, the molten region at the time instant t must be computed from the temperature profile, so the solution of the thermal problem is needed to solve the hydrodynamic problem. We will see below how the domain $\Omega_l(t)$ is determined to carry out the numerical simulation.

The right-hand side term $\mathbf{f}$ contains the forces supported by the fluid due to natural convection (buoyancy forces, $\mathbf{f}_g$) and those due to the electromagnetic field (Lorentz forces, $\mathbf{f}_l$):

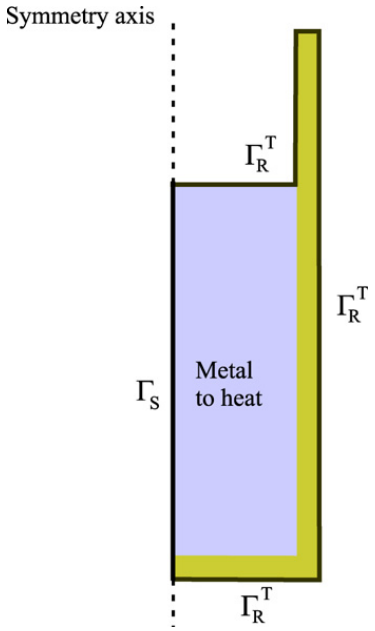

Fig. 4. Computational domain for the thermal problem.

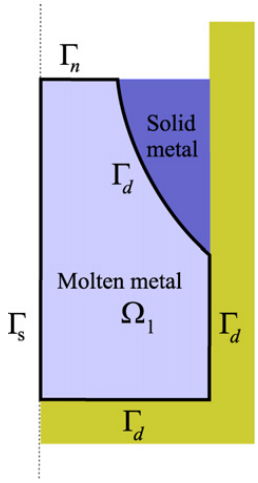

Fig. 5. Computational domain for the hydrodynamic problem.

$$\mathbf{f} = \mathbf{f}_g(\mathbf{x}, T) + \mathbf{f}_l(\mathbf{x}) \tag{58}$$

with

$$\mathbf{f}_g = \rho(\mathbf{x}, T)\mathbf{g}, \tag{59}$$

$$\mathbf{f}_l = \frac{\omega}{2\pi} \int_0^{2\pi/\omega} \mathcal{J}(\mathbf{x}, t) \times \mathcal{B}(\mathbf{x}, t)\, dt, \tag{60}$$

where $\mathbf{g}$ denotes the acceleration of gravity, ω is the angular frequency, and $\mathcal{J}$ and $\mathcal{B}$ are the current density and the magnetic induction fields, respectively.

Eqs. (56), (57) are completed with the following initial and boundary conditions

$$\mathbf{u} = \mathbf{0} \quad \text{on } \Gamma_d(t), \tag{61}$$

$$S\mathbf{n} = \mathbf{0} \quad \text{on } \Gamma_n(t), \tag{62}$$

$$S\mathbf{n} = \mathbf{0} \quad \text{on } \Gamma_s(t), \tag{63}$$

$$\mathbf{u} = \mathbf{0} \quad \text{in } \Omega_l(0), \tag{64}$$

where S denotes the Cauchy stress tensor, $S = -pI + 2\eta D(\mathbf{u})$, and I is the identity tensor

4.1. Boussinesq approximation

As the range of temperatures in the molten region is not very large, we can use the Boussinesq approximation to model the fluid motion. This approximation basically consists in modifying the Navier–Stokes equations by taking a certain reference temperature, and considering the constant values of density and viscosity at this temperature for the inertial and dissipative terms, while a linear temperature-dependent density is considered in the right-hand side. That is,

$$\rho_0\left(\frac{\partial \mathbf{u}}{\partial t} + (\mathbf{grad}\,\mathbf{u})\,\mathbf{u}\right) - \operatorname{div}\big(2\eta_0 D(\mathbf{u})\big) + \mathbf{grad}\,p' = -\rho_0\beta_0(T - T_0)\mathbf{g} + \mathbf{f}_l, \tag{65}$$

$$\operatorname{div}\mathbf{u} = 0, \tag{66}$$

where ρ_0 and η_0 denotes the density and the dynamic viscosity at the reference temperature, respectively, β_0 is the coefficient of thermal expansion, and p' is a modified pressure, such that $\mathbf{grad}\,p' = \mathbf{grad}\,p - \rho_0\mathbf{g}$.

The heat equation is also modified in a similar form, to obtain

$$\rho_0 c_{p0}\left(\frac{\partial T}{\partial t} + \mathbf{u}\cdot\mathbf{grad}\,T\right) - \operatorname{div}(k_0\,\mathbf{grad}\,T) = \frac{|\mathbf{J}|^2}{2\sigma}, \tag{67}$$

where c_{p0} represents the specific heat at the reference temperature, and k_0 the thermal conductivity at the same temperature. We remark that this approximation for the thermal model is only used in the molten region of the metal. In the rest of the domain the heat equation remains non-linear.

4.2. An algebraic turbulence model: Smagorinsky's model

We recall that the Reynolds number is a dimensionless quantity which gives the ratio of inertial forces to viscosity forces. It is expressed as

$$Re = \frac{\rho U L}{\eta}, \tag{68}$$

where U and L represent a characteristic velocity and a characteristic length (here taken as the inner radius of the crucible), respectively. When this number goes beyond a threshold, the flow becomes turbulent, and then it is impossible to model its behavior using the Navier–Stokes equations due to the big mesh size that the computational domain would require. To deal with turbulent flows, all the fields are decomposed into a mean part and an oscillating part which takes into account the small variations due to turbulent flow. By rewriting the Navier–Stokes equations using the decomposed fields, and filtering the equations (see [23]) we arrive to the Reynolds-averaged Navier–Stokes equations:

$$\rho_0\left(\frac{\partial \hat{\mathbf{u}}}{\partial t} + (\mathbf{grad}\,\hat{\mathbf{u}})\,\hat{\mathbf{u}}\right) - \operatorname{div}\big(2\eta_0 D(\hat{\mathbf{u}})\big) - \rho_0 \operatorname{div}\widehat{\mathbf{u}'\otimes\mathbf{u}'} + \mathbf{grad}\,\hat{p} = \hat{\mathbf{f}} \quad \text{in } \Omega_l(t), \tag{69}$$

$$\operatorname{div}\hat{\mathbf{u}} = 0 \quad \text{in } \Omega_l(t), \tag{70}$$

where $\hat{\mathbf{u}}$ denotes the mean velocity, $\hat{p}$ the mean pressure, $\mathbf{u}'$ the oscillating part of the velocity field and $\otimes$ the tensor product. Hereafter, the symbol $\hat{}$ denotes the mean value of a variable or an expression. The term $R = \rho_0(\widehat{\mathbf{u}'\otimes\mathbf{u}'})$ is called the Reynolds tensor and represents the contribution of the turbulent part to the mean flow.

Analogously, the averaged heat equation is written as

$$\rho_0 c_{p0}\left(\frac{\partial \hat{T}}{\partial t} + \hat{\mathbf{u}}\cdot\mathbf{grad}\,\hat{T}\right) + \rho_0 c_{p0}\operatorname{div}\widehat{T'\mathbf{u}'} - \operatorname{div}(k_0\,\mathbf{grad}\,\hat{T}) = \frac{\widehat{|\mathbf{J}|^2}}{2\sigma}, \tag{71}$$

being $\hat{T}$ the mean temperature and T' its oscillating part. The tensor $\rho_0 c_{p0}\widehat{T'\mathbf{u}'}$ takes into account the contribution of the turbulent flow to the mean temperature profile.

The Boussinesq assumption consists in taking these two tensors as

$$-\rho_0\widehat{\mathbf{u}'\otimes\mathbf{u}'} = -\frac{1}{3}\operatorname{tr}(R)I + 2\eta_t D(\hat{\mathbf{u}}), \tag{72}$$

$$\rho_0 c_{p0}\widehat{T'\mathbf{u}'} = -k_t\,\mathbf{grad}\,\hat{T}, \tag{73}$$

where η_t is the turbulent viscosity, k_t is the turbulent thermal conductivity and $\operatorname{tr}(\cdot)$ denotes the trace operator. Using this assumption we can now rewrite Eqs. (69) and (71) as

$$\rho_0\left(\frac{\partial \hat{\mathbf{u}}}{\partial t} + (\mathbf{grad}\,\hat{\mathbf{u}})\,\hat{\mathbf{u}}\right) - \operatorname{div}\big(2\eta_{\text{eff}} D(\hat{\mathbf{u}})\big) + \mathbf{grad}\,\hat{p}^* = \hat{\mathbf{f}}, \tag{74}$$

$$\rho_0 c_{p0}\left(\frac{\partial \hat{T}}{\partial t} + \hat{\mathbf{u}}\cdot\mathbf{grad}\,\hat{T}\right) - \operatorname{div}(k_{\text{eff}}\,\mathbf{grad}\,\hat{T}) = \frac{\widehat{|\mathbf{J}|^2}}{2\sigma}, \tag{75}$$

where $p^* = p' - \frac{1}{3}\operatorname{tr}(R)$ and η_{eff} is the effective viscosity, which is given by $\eta_{\text{eff}} = \eta_0 + \eta_t$. Analogously, k_{eff} represents the effective thermal conductivity, given by $k_{\text{eff}} = k_0 + k_t$. Different models are obtained depending on the way in which the turbulent viscosity η_t and the turbulent conductivity k_t are computed. An efficient and easy to implement model is the one proposed by Smagorinsky (see [23]), which consists in considering

$$\eta_t = \rho_0 c h^2\big|D(\hat{\mathbf{u}})\big|, \quad c \cong 0.01, \qquad k_t = c_{p0}\frac{\eta_t}{Pr_t}, \tag{76}$$

where $h(x)$ is the mesh size of the numerical method around point x, and Pr_t is the turbulent Prandtl number, which is taken equal to 0.9 (see [23]).

5. Numerical solution

In this section we introduce a weak formulation and a time-space discretization of the coupled problem as well as the determination of the hydrodynamic domain. Again, we will exploit the cylindrical symmetry of the domain when solving the hydrodynamic problem. We notice that $\mathbf{u}$ does not depend on θ and it has zero component in the tangential direction $\mathbf{e}_\theta$. In order to simplify, in what follows we shall drop index θ for A_θ and J_θ, and index t for $\Omega_l(t)$. We shall also drop the superindex notation $\hat{}$ for the filtered fields and terms.

5.1. Computation of the hydrodynamic domain

As said before, the region occupied by the molten material varies over time, and depends on temperature. We consider a fixed mesh of the region occupied by the metal to be heated, i.e., the solid and molten metal in Fig. 5. At each time step, in order to determine the hydrodynamic domain, we need to compute the position of the boundary of the molten region. To do that, we are obliged to solve the thermal problem previously. More precisely, the enthalpy profile given by the solution of problem **(WTP)** introduced in Section 5.3, allows us to choose those elements of the mesh belonging to the liquid region. The hydrodynamic computational mesh is then updated. We notice that the mushy region, that is, the region where the melting temperature has been reached but the material is not completely molten, is not considered as a part of the hydrodynamic domain.

5.2. Time discretization

To obtain a suitable discretization of the material time derivative in Eqs. (53) and (56) we shall use the characteristics method (see [26]). We will only explain the discretization for the material derivative of the enthalpy since the same holds for the velocity $\mathbf{u}$.

Given a velocity field $\mathbf{u}$ we define the characteristic curve going through point $\mathbf{x}$ at time t as the solution of the following Cauchy problem

$$\begin{cases} \dfrac{\mathrm{d}}{\mathrm{d}\tau}\mathbf{X}(\mathbf{x},t;\tau) = \mathbf{u}\big(\mathbf{X}(\mathbf{x},t;\tau),\tau\big), \\ \mathbf{X}(\mathbf{x},t;t) = \mathbf{x}, \end{cases} \tag{77}$$

so $\mathbf{X}(\mathbf{x},t;\tau)$ is the trajectory of the material point being at position $\mathbf{x}$ at time t. The material time derivative of e is defined by

$$\dot{e}(\mathbf{x},t) = \frac{d}{d\tau}\big[e\big(\mathbf{X}(\mathbf{x},t;\tau),\tau\big)\big]_{|\tau=t}. \tag{78}$$

We consider a time interval $[0,t_f]$ and a discretization time step $\Delta t = t_f/N$, to obtain a uniform partition of the interval $\Pi = \{t^n = n\Delta t, 0 \leqslant n \leqslant N\}$. Let e^n and $\mathbf{u}^n$ be the approximations of e and $\mathbf{u}$ at time t^n, respectively. We approximate the material time derivative of e at time t^{n+1} by

$$\dot{e}\big(\mathbf{x},t^{n+1}\big) \simeq \frac{e^{n+1}(\mathbf{x}) - e^n(\chi^n(\mathbf{x}))}{\Delta t}, \tag{79}$$

where $\chi^n(\mathbf{x}) = \mathbf{X}^n(\mathbf{x},t^{n+1};t^n)$ is obtained as the solution of the following Cauchy problem

$$\begin{cases} \dfrac{\mathrm{d}}{\mathrm{d}\tau}\mathbf{X}^n\big(\mathbf{x},t^{n+1};\tau\big) = \mathbf{u}^n\big(\mathbf{X}^n\big(\mathbf{x},t^{n+1};\tau\big),\tau\big), \\ \mathbf{X}^n\big(\mathbf{x},t^{n+1};t^{n+1}\big) = \mathbf{x}, \end{cases} \tag{80}$$

backward in time. Notice that, since $\mathbf{u} = \mathbf{0}$ in the solid region, the solution of this Cauchy problem is $\mathbf{X}^n(\mathbf{x},t^{n+1};\tau) = \mathbf{x}$ for any τ, and so Eq. (79) in the solid part is equivalent to a standard time discretization without using the method of characteristics. Analogously to (79), the material time derivative of the velocity at time t^{n+1} is approximated by

$$\dot{\mathbf{u}}\big(\mathbf{x},t^{n+1}\big) \simeq \frac{\mathbf{u}^{n+1}(\mathbf{x}) - \mathbf{u}^n(\chi^n(\mathbf{x}))}{\Delta t}. \tag{81}$$

5.3. Weak formulation

If we consider in (74) the discretization for the material time derivative of $\mathbf{u}$ introduced above, then, taking into account the cylindrical symmetry, multiplying Eqs. (74) and (70) by suitable test functions, and integrating in the liquid domain Ω_l we obtain, after using the Green's formula, the following weak formulation of the semi-discretized hydrodynamic problem

Problem WHP. For each $n = 0,1,\ldots,M-1$, find functions $\mathbf{u}^{n+1}$ and p^{n+1} such that $\mathbf{u}^{n+1} = 0$ on Γ_d and furthermore

$$\begin{aligned} &\frac{1}{\Delta t}\int_{\Omega_l} \rho_0 \mathbf{u}^{n+1}\cdot\mathbf{w} r\,dr\,dz + \int_{\Omega_l} \eta_{\mathrm{eff}}\big(\mathbf{grad}\,\mathbf{u}^{n+1} : \mathbf{grad}\,\mathbf{w}\big) r\,dr\,dz \\ &\quad + \int_{\Omega_l} \eta_{\mathrm{eff}}\big(\big(\mathbf{grad}\,\mathbf{u}^{n+1}\big)^t : \mathbf{grad}\,\mathbf{w}\big) r\,dr\,dz - \int_{\Omega_l} p^{n+1}\,\mathrm{div}\,\mathbf{w} r\,dr\,dz \\ &= \int_{\Omega_l} \mathbf{f}_g^{n+1}\cdot\mathbf{w} r\,dr\,dz + \int_{\Omega_l} \mathbf{f}_l^{n+1}\cdot\mathbf{w} r\,dr\,dz + \frac{1}{\Delta t}\int_{\Omega_l} \rho_0\big(\mathbf{u}^n\circ\chi^n\big)\cdot\mathbf{w} r\,dr\,dz, \end{aligned}$$

$$\int_{\Omega_l} \operatorname{div} \mathbf{u}^{n+1} q r\,dr\,dz = 0,$$

for all test functions $\mathbf{w}$ null on Γ_d and q.

The notation $(\cdot:\cdot)$ represents the scalar product of two tensors. Similarly, if we multiply Eq. (53) discretized in time by a test function, after using a Green's formula we obtain the following weak formulation of the semi-discretized thermal problem:

Problem WTP. For each $n = 0, 1, \ldots, M-1$, find a function T^{n+1} such that

$$\begin{aligned}
&\int_{\Omega_0} \frac{1}{\Delta t} e^{n+1} Z r\,dr\,dz + \int_{\Omega_0} k_{\mathrm{eff}}\big(r, z, T^{n+1}\big)\,\mathbf{grad}\, T^{n+1} \cdot \mathbf{grad}\, Z r\,dr\,dz \\
&\quad = \int_{\Gamma_{\mathrm{R}}^{\mathrm{T}}} \big(\alpha\big(T_c - T^{n+1}\big) + \gamma\big(T_r^4 - \big(T^{n+1}\big)^4\big)\big) Z r\,d\Gamma + \int_{\Omega_0} \frac{1}{\Delta t}\big(e^n \circ \chi^n\big) Z r\,dr\,dz + \int_{\Omega_0} \frac{1}{2\sigma\big(r, z, T^{n+1}\big)} \big|J^{n+1}\big|^2 Z r\,dr\,dz, \qquad (82)
\end{aligned}$$

for all test function Z.

Finally, an approximation of field A at time t^{n+1} is determined as the solution of the weak formulation obtained in Section 2:

Problem WEP. Given $\mathbf{I} = (I_1, \ldots, I_m) \in \mathbb{C}^m$, find $A' : \Omega \to \mathbb{C}$, $\mathbf{V} \in \mathbb{C}^m$ and $\lambda' : \Gamma \to \mathbb{C}$ such that

$$\begin{aligned}
&\mathrm{i}\omega \int_{\Omega} \frac{\sigma\big(r, z, T^{n+1}\big)}{r} A' \bar{\psi}'\,dr\,dz + \int_{\Omega} \frac{1}{\mu\big(r, z, T^{n+1}\big) r}\,\mathbf{grad}\, A' \cdot \mathbf{grad}\, \bar{\psi}'\,dr\,dz \\
&\quad - \int_{\Gamma} \frac{1}{\mu\big(r, z, T^{n+1}\big) r} \lambda' \bar{\psi}'\,d\gamma + \sum_{k=1}^{m} \frac{V_k}{2\pi} \int_{\Omega_k} \frac{\sigma\big(r, z, T^{n+1}\big)}{r} \bar{\psi}'\,dr\,dz = 0, \quad \forall \psi', \\
&\frac{1}{2\pi} \sum_{k=1}^{m} \bar{W}_k \int_{\Omega_k} \frac{\sigma\big(r, z, T^{n+1}\big)}{r} A'\,dr\,dz + \frac{1}{4\pi^2 \mathrm{i}\omega} \sum_{k=1}^{m} \bar{W}_k \int_{\Omega_k} \sigma\big(r, z, T^{n+1}\big) \frac{V_k}{r}\,dr\,dz = -\frac{1}{2\pi\,\mathrm{i}\omega} \sum_{k=1}^{m} I_k \bar{W}_k, \quad \forall \mathbf{W} \in \mathbb{C}^m, \\
&\int_{\Gamma} \frac{1}{\mu\big(r, z, T^{n+1}\big) r}\,\bar{\zeta} A' - \int_{\Gamma} \frac{1}{\mu\big(r, z, T^{n+1}\big)} (\mathcal{G}_n A') \bar{\zeta}(r, z)\,d\gamma + \int_{\Gamma} \frac{1}{\mu\big(r, z, T^{n+1}\big)} (\mathcal{G}\lambda') \bar{\zeta}(r, z)\,d\gamma = 0 \quad \forall \zeta.
\end{aligned}$$

5.4. Space discretization

Problem **WTP** has been spatially discretized by a piecewise linear finite element method defined in a triangular mesh of the workpiece domain Ω_0. On the other hand problem **WEP** has been spatially discretized by a finite and boundary element method (see [8] for further details). Problem **WHP** has been spatially discretized by the finite element couple P_1-*bubble*/P_1, which is known to satisfy the *inf-sup* condition (see, for instance, [12]). We should also remark that the hydrodynamic problem is only solved in the liquid domain Ω_l, which must be computed at each time step.

We notice that, at each time step, the three problems form a coupled non-linear system. In the thermal problem the heat source depends on the solution of the electromagnetic problem, while the convective heat transfer needs the solution of the hydrodynamic problem. Also, the Lorentz force in the hydrodynamic problem depends on the solution of the electromagnetic problem. On the other hand, parameters k, σ, μ, ρ and η depend on temperature. The radiation–convection boundary condition in the thermal problem depends on T^4. To handle the coupling between the three problems and in order to deal with the non-linearities in the enthalpy and the radiation–convection boundary condition, we propose a fixed point algorithm which is described in Fig. 6 (see [6] and [7] for the details). Note that the thermal problem only needs the solution of the hydrodynamic problem at the previous time step. Since we are neglecting velocity in Ohm's law, we are allowed to solve the hydrodynamic problem segregated from the two others.

6. Numerical results

In this section we present some numerical results which have been obtained by using the computer code THESIF (http://www.usc.es/~thesif/) implementing the algorithm introduced above. Two different cases are considered: the former is a comparison of the results of the axisymmetric code with the analytical solution of an academic problem. The latter is the numerical simulation of an industrial furnace.

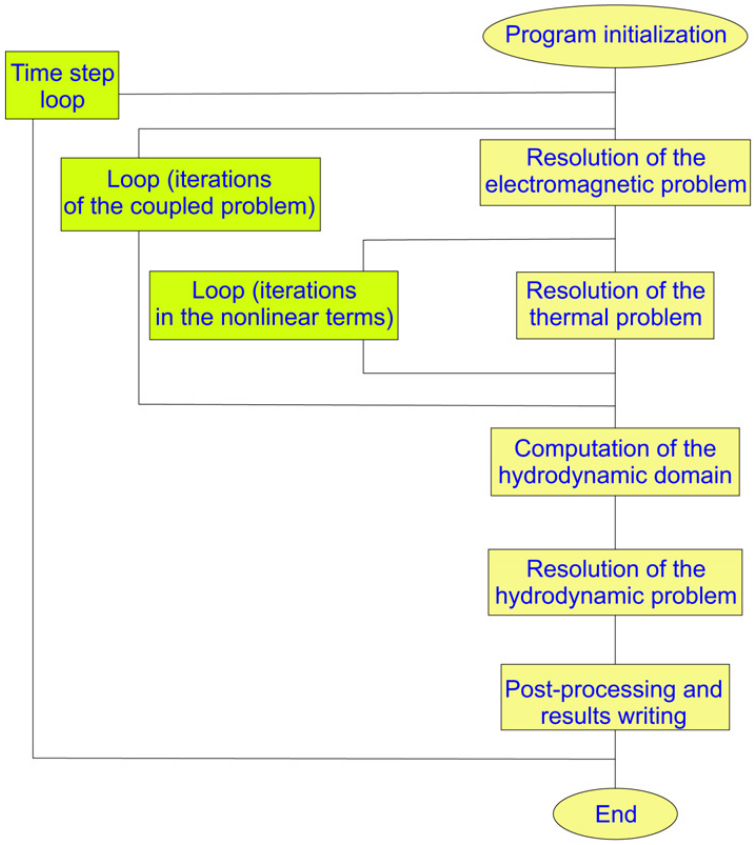

Fig. 6. Scheme of the algorithm.

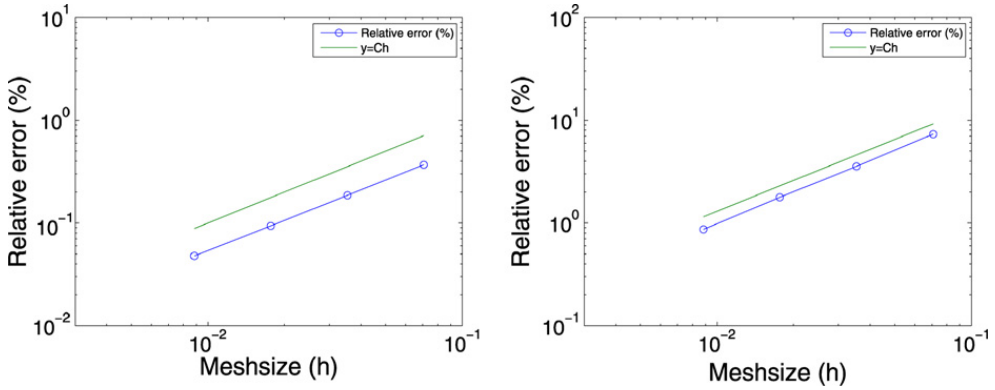

Fig. 7. Error versus meshsize (log–log scale). Fields T (left) and $\mathbf{u}$ (right).

6.1. Academic test

The thermo-electrical problem stated in this paper has already been tested by the authors in a previous work (see [7]). That is why in this paper we only test the thermo-hydrodynamic problem with phase change, by comparing the numerical results with the analytical solution of the academic problem introduced below (see Appendix A for a more extensive description). This problem consists of a solid ball of exponentially decreasing radius and a liquid region outside the ball.

Since the velocity is now the solution of a steady equation, the code has been slightly modified to solve the correct problem, and time discretization is no longer used for the hydrodynamic problem. Therefore, gravity and Lorentz force are not taken into account.

The numerical method has been used on several successively refined two-dimensional meshes, and the numerical results obtained have been compared with the analytical solution. We have computed the error in L^{∞} (in time)–L^2 (in space) norm. Fig. 7 shows the log–log plots of the errors for the computed temperature T and velocity $\mathbf{u}$, respectively, versus the meshsize h, where we can observe a linear dependence on this parameter.

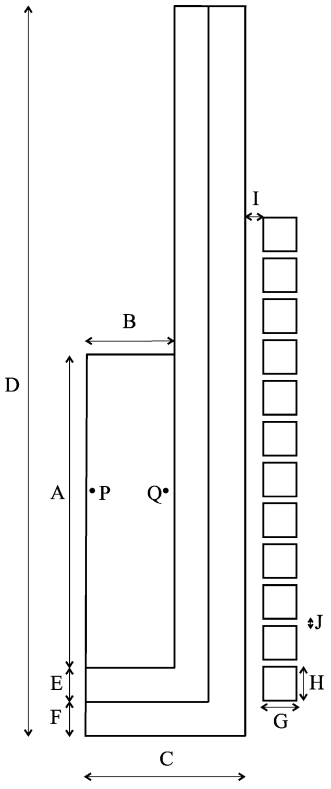

Fig. 8. Sketch of the geometry.

Table 1
Geometrical data.

A. Height of silicon	0.45 m
B. Inner radius of crucible	0.125 m
C. Outer radius of crucible	0.225 m
D. Crucible height	1.05 m
E. Crucible width	0.05 m
F. Alumina layer width	0.05 m
G. Turn diameter	0.05 m
H. Turn height	0.05 m
I. Distance between coil and crucible	0.025 m
J. Distance between the turns	0.01 m
Number of coil turns	12
P, Q. Measure points	

Table 2
Operating parameters for each simulation.

Simulation	Frequency (Hz)	RMS coil current (A)
1	100	5500
2	1000	2000

6.2. Industrial furnace

In this case we have applied the algorithm to simulate an industrial furnace used for silicon purification. The workpiece we are considering consists of a graphite crucible containing silicon to be melted and surrounded by an alumina layer to avoid heat losses through the boundary. The initial temperature of the workpiece is 30 °C. The induction coil is made with copper. As we detailed in Section 2, the thermal model has been simplified and does not include the coil. The geometrical data of this furnace are summarized in Fig. 8 and Table 1. A detail of the computational mesh can be seen in Fig. 9. The physical properties of the three materials in the workpiece depend on temperature and have been obtained from literature while, in the coil, the electromagnetic parameters are supposed to be constant.

Two different simulations have been carried out varying current frequency and intensity. The physical parameters for each simulation are detailed in Table 2.

Figs. 10 and 11 show the temperature field in the workpiece for both simulations and at 30 minutes and 150 minutes from the beginning. Figs. 12 and 13 show the modulus of current density for both simulations and at the same times.

Note that at low frequencies the skin-depth is higher, and so the electromagnetic field penetrates deeper into the workpiece, as can be seen in Fig. 13. This causes electromagnetic stirring in the molten silicon due to Lorentz force. At higher frequencies, Lorentz force concentrates near the graphite crucible, and so buoyancy forces become more important (see Fig. 14).

Fig. 15 illustrates the importance of considering heat transfer when computing the temperature field. One can check how neglecting the convection term in the heat equation could cause the materials to reach very high and unrealistic temperatures that would originate the crucible to melt.

We complete these results by representing, in Figs. 16 and 17, the evolution in time of the temperature and the current density for both simulations and for two different points in the silicon: a point P close to the symmetry axis and a point Q close to the graphite crucible. As can be seen from Fig. 16, at low frequency, when Lorentz forces dominate, the temperature profile is quite stable reaching almost a steady state. However, at higher frequencies, when buoyancy forces become more important, the solution does not reach the steady state but it varies in a sort of periodic way. The big variations in the

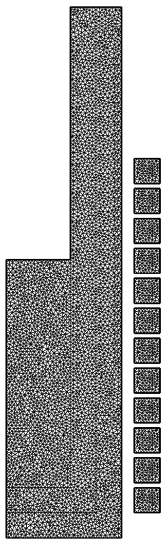

Fig. 9. Detail of the mesh.

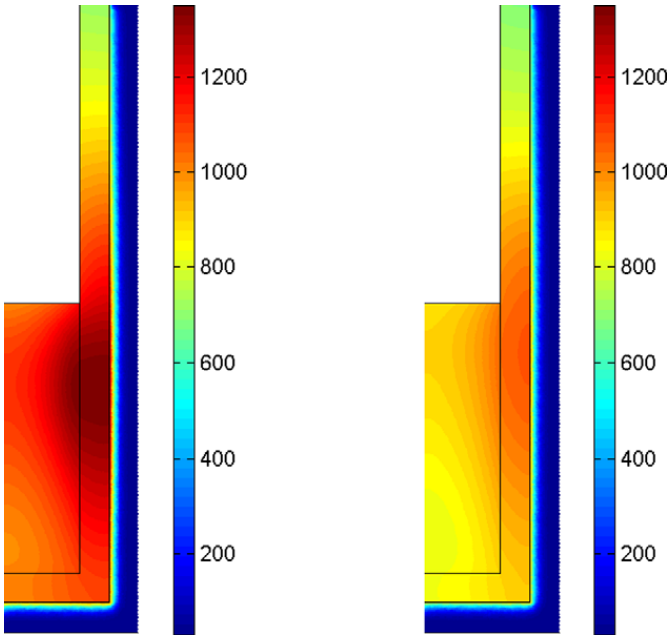

Fig. 10. Temperature at time $t = 30$ min for simulation 1 (left) and 2 (right).

current density magnitude are due to the fact that solid silicon is a dielectric whereas molten silicon is a good electrical conductor. These graphics also confirm the fact that the lower the frequency the larger the skin-depth.

Finally, Fig. 18 shows the velocity fields at time 150 minutes for each of the simulations. We can appreciate the swirls due to Lorentz forces.

Acknowledgements

The authors wish to thank Professor Rodolfo Rodríguez for many useful discussions on the electromagnetic problem. They also express their gratitude to the referees for their useful remarks.

Appendix A. Analytical solution of a thermo-hydrodynamic problem with phase change

In this section we present a simplified problem having an analytical solution which has been used for the validation of the code. Due to the difficulty in obtaining a problem with analytical solution for the whole coupled equations, and since the velocity field has no influence on the electromagnetic problem, we are just considering a thermo-hydrodynamic problem with phase change. This problem is an adaptation of another one used in [10] for the same purpose of validation.

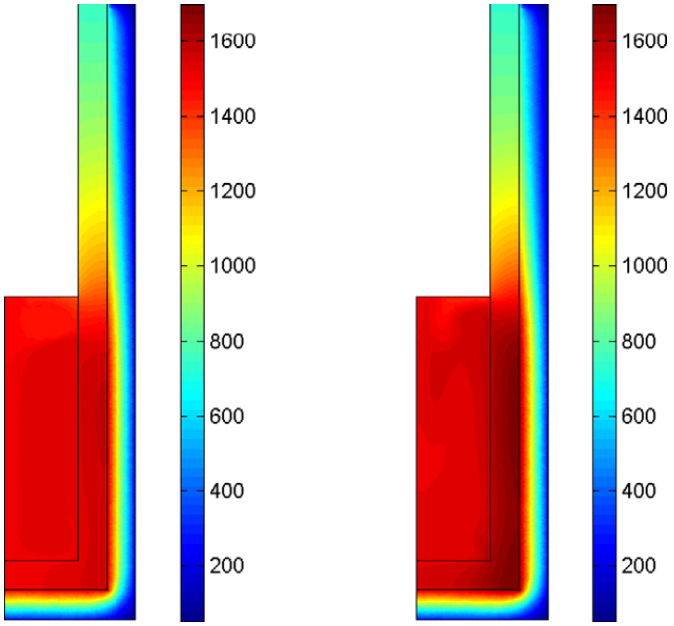

Fig. 11. Temperature at time $t = 150$ min for simulation 1 (left) and 2 (right).

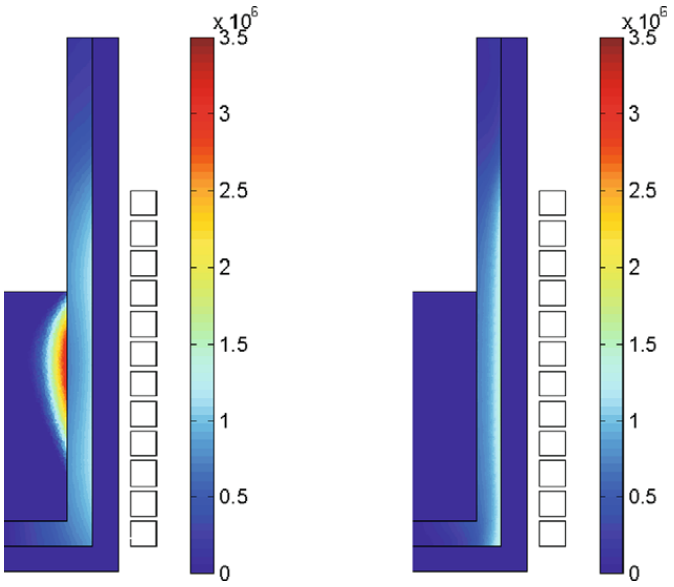

Fig. 12. Modulus of current density at time $t = 30$ min for simulation 1 (left) and 2 (right).

We take $t_f = 1$ as the final time. The spatial domain we consider is given, in cylindrical coordinates, by $\Omega = (0,1) \times (0, 2\pi) \times (-1, 1)$.

For each time t we define the function

$$g(r,z,t) = r^2 + z^2 - 0.25e^{-t}, \tag{A.1}$$

and we suppose the temperature is given by

$$T(r,z,t) = \begin{cases} 2g(r,z,t) + 1, & \text{if } g(r,z,t) \geqslant 0, \\ g(r,z,t) + 1, & \text{if } g(r,z,t) < 0. \end{cases} \tag{A.2}$$

The temperature defined in this way is a continuous function. The phase change temperature is $T_s = 1$, and so the free boundary between the solid and the liquid region is given by

$$S(t) = \left\{ \mathbf{x} = (r,\theta,z) \mid r^2 + z^2 = 0.25e^{-t} \right\}, \tag{A.3}$$

that is, the solid region is the ball centered at the origin and radius $0.5e^{-0.5t}$.

The thermophysical parameters considered are $\rho(T) = 1$, $k(T) = 1$ and

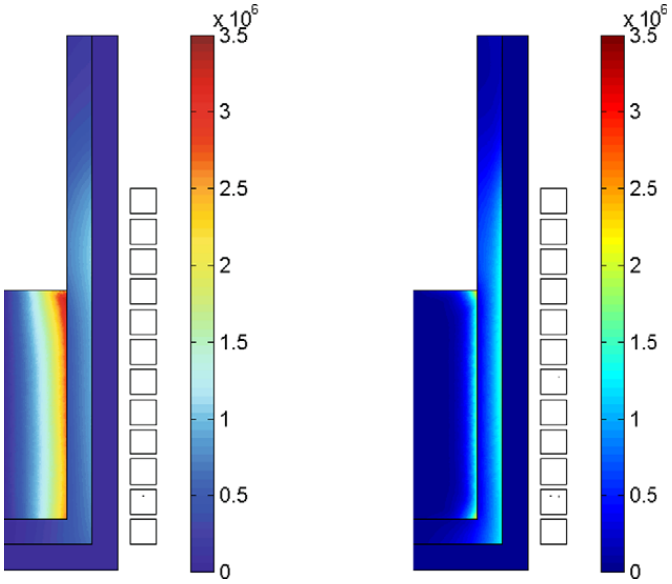

Fig. 13. Modulus of current density at time $t = 150$ min for simulation 1 (left) and 2 (right).

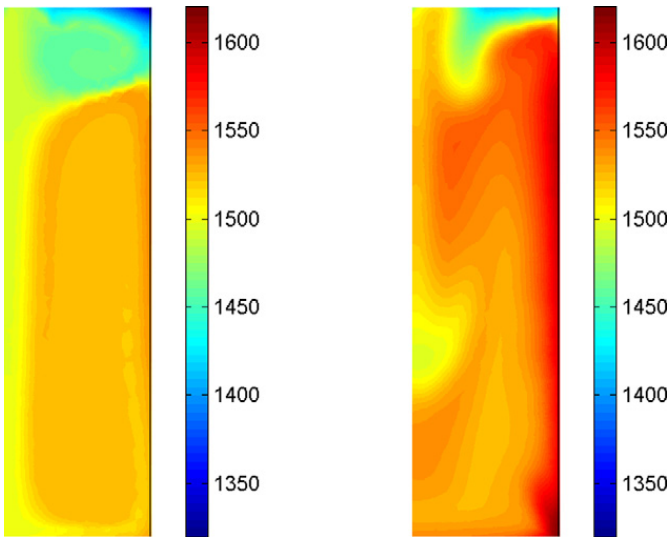

Fig. 14. Silicon temperature at time $t = 150$ min for simulation 1 (left) and 2 (right).

$$c(T) = \begin{cases} 2, & \text{if } T \leqslant 1, \\ 6, & \text{if } T > 1, \end{cases} \tag{A.4}$$

i.e., the density and the thermal conductivity are constant, while the specific heat is constant on each phase separately. The latent heat is $L = 4$.

As we mentioned above, the temperature T is a continuous function, but $\mathbf{grad}\, T$ is discontinuous across the interphase $S(t)$. It can be seen that for the parameters and the function T given before, the Stefan condition on the interphase is satisfied. This condition is expressed by the following equality

$$\left[k(T)\frac{\partial T}{\partial \mathbf{n}}\right] = \rho L \mathbf{U} \cdot \mathbf{n}, \tag{A.5}$$

where $[\varphi]$ denotes the jump of function φ through the interphase, $\mathbf{n}$ is the unit vector normal to the interphase $S(t)$ outward to the solid region and $\mathbf{U}$ is the velocity of the interphase advance.

For the thermal problem we consider Eq. (52), substituting the heat source from the Joule effect by a function f

$$\left(\frac{\partial e}{\partial t} + \mathbf{u} \cdot \mathbf{grad}\, e\right) - \operatorname{div}\big(k(\mathbf{x}, T)\, \mathbf{grad}\, T\big) = f \quad \text{in } \Omega, \tag{A.6}$$

where f is

$$f(r, z, t) = \begin{cases} 3e^{-t} - 12 + \mathbf{u} \cdot (24r, 24z), & \text{if } g(r, z, t) \geqslant 0, \\ 0.5e^{-t} - 6, & \text{if } g(r, z, t) < 0. \end{cases}$$

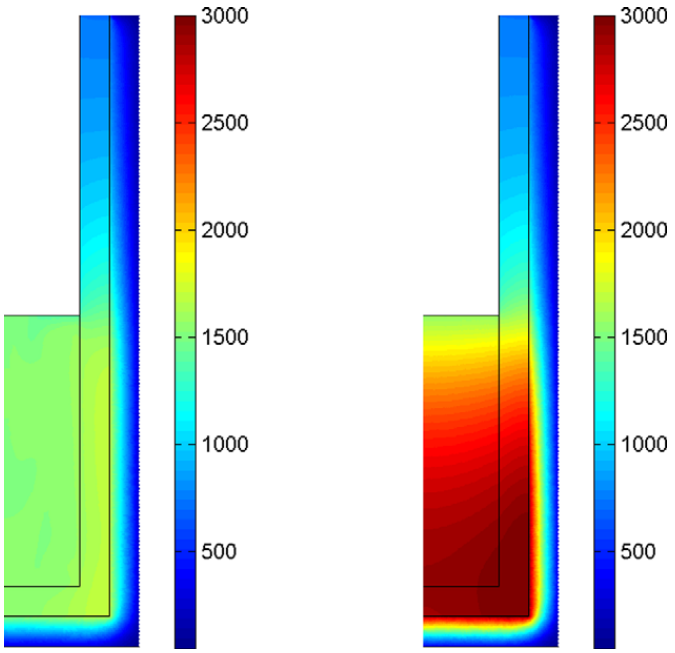

Fig. 15. Temperature at time $t = 150$ min for simulation 2 with and without convection.

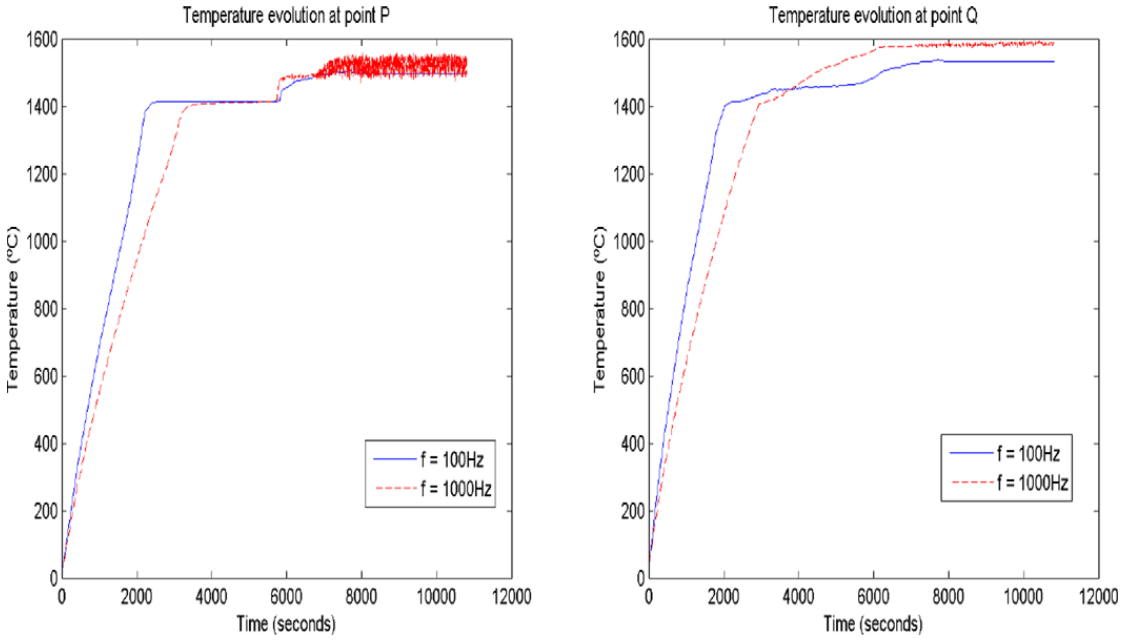

Fig. 16. Evolution of temperature at points P and Q.

For the boundary condition in (55) we have taken $\alpha = 0$ and $\gamma = 1$ so that only the radiation condition is taken into account, namely

$$k\frac{\partial T}{\partial \mathbf{n}} = T_r^4 - T^4, \tag{A.7}$$

If we replace in this equation the value of T given in (A.2), we conclude that

$$T_r = \sqrt[4]{\big(2g(r,z,t)+1\big)^4 + k\mathbf{n}\cdot(r,z)}, \tag{A.8}$$

where $\mathbf{n}$ is the outward unit normal vector to the boundary and k is the thermal conductivity which is equal to 1.

Finally, we must define a velocity field in the liquid region. We choose the Stokes' flow around the sphere occupied by the solid region. We recall that this flow is the solution of the Stokes stationary equations

$$-\eta\Delta\mathbf{u} + \mathbf{grad}\, p = \mathbf{0}, \tag{A.9}$$

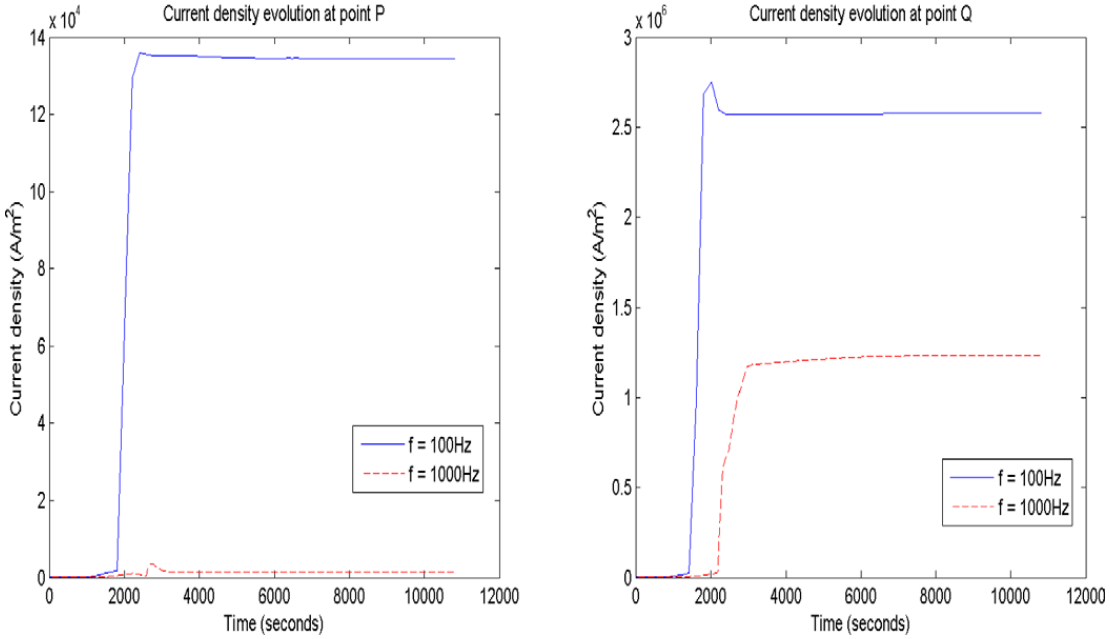

Fig. 17. Evolution of current density at points P and Q.

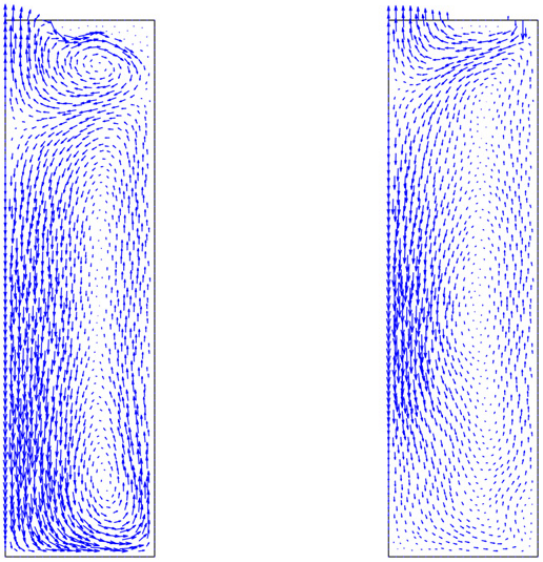

Fig. 18. Velocity field at $t = 150$ min for simulation 1 (left) and 2 (right).

$$\operatorname{div} \mathbf{u} = 0, \tag{A.10}$$

where Eq. (A.9) corresponds to the motion equation for low Reynolds number. The velocity field we are interested in is the solution of (A.9)–(A.10) together with conditions

$$\mathbf{u} = \mathbf{0} \quad \text{on } r = R, \tag{A.11}$$

$$\mathbf{u} = u\mathbf{e}_3, \quad p = p_\infty \quad \text{at } r \to \infty, \tag{A.12}$$

where R is the radius of the ball containing the solid region and u is a constant representing the velocity at infinity.

To solve the problem, we take into account that the dynamic viscosity is constant and equal to one, $\eta = 1$. Then the velocity field which is the solution of Eqs. (A.9)–(A.12) can be expressed in cylindrical coordinates as follows:

$$\begin{aligned} u_r &= \frac{3u}{4}\frac{rz}{r^2+z^2}\left(\frac{R^3}{(r^2+z^2)^{3/2}} - \frac{R}{(r^2+z^2)^{1/2}}\right), \\ u_z &= \frac{3u}{4}\frac{z^2}{r^2+z^2}\left(\frac{R^3}{(r^2+z^2)^{3/2}} - \frac{R}{(r^2+z^2)^{1/2}}\right) + u\left(1 - \frac{3R}{4(r^2+z^2)^{1/2}} - \frac{R^3}{4(r^2+z^2)^{3/2}}\right). \end{aligned} \tag{A.13}$$

In our case we will take $R = R(t)$ as the radius of the ball containing the solid region at instant t, i.e., $R(t) = 0.5e^{-0.5t}$.

In the hydrodynamic problem we impose Dirichlet boundary conditions, taking $\mathbf{u}$ as given in (A.13) in the boundary of the box surrounding the ball, and $\mathbf{u} = 0$ on the ball.

References

[1] A.M. Alonso Rodríguez, A. Valli, Mixed finite element approximation of eddy current problems based on the electric field, in: P. Neittaanmäki, T. Rossi, K. Majava, O. Pironneau (Eds.), ECCOMAS 2004: European Congress on Computational Methods in Applied Sciences and Engineering, University of Jyväskylä, Department of Mathematical Information Technology, Jyväskylä, 2004.

[2] A.M. Alonso Rodríguez, A. Valli, Voltage and current excitation for time-harmonic eddy-current problems, Preprint UTM 716, Università di Trento. Dipartimento di Matematica, 2007.

[3] C. Amrouche, C. Bernardi, M. Dauge, V. Girault, Vector potentials in three-dimensional non-smooth domains, Math. Meth. Appl. Sci. 21 (1998) 823–864.

[4] H. Ammari, A. Buffa, J.C. Nédélec, A justification of eddy currents model for the Maxwell equations, SIAM J. Appl. Math. 60 (5) (2000) 1805–1823.

[5] F. Bay, V. Labbe, Y. Favennec, J.L. Chenot, A numerical model for induction heating processes coupling electromagnetism and thermomechanics, Int. J. Numer. Meth. Engrg. 5 (2003) 839–867.

[6] A. Bermúdez, J. Bullón, F. Pena, P. Salgado, A numerical method for transient simulation of metallurgical compound electrodes, Finite Elem. Anal. Des. 39 (2003) 283–299.

[7] A. Bermúdez, D. Gómez, M.C. Muñiz, P. Salgado, Transient numerical simulation of a thermoelectrical problem in cylindrical induction heating furnaces, Adv. Comput. Math. 26 (2007) 39–62.

[8] A. Bermúdez, D. Gómez, M.C. Muñiz, P. Salgado, A FEM/BEM for axisymmetric electromagnetic and thermal modelling of induction furnaces, Internat. J. Numer. Methods Engrg. 71 (7) (2007) 856–882.

[9] A. Bermúdez, R. Leira, M.C. Muñiz, F. Pena, Numerical modelling of a transient conductive-radiative thermal problem arising from silicon purification, Finite Elem. Anal. Des. 42 (2006) 809–820.

[10] A. Bermúdez, M.V. Otero Piñeiro, Numerical solution of a three-dimensional solidification problem in aluminium casting, Finite Elem. Anal. Des. 40 (2004) 1885–1906.

[11] A. Bossavit, Computational Electromagnetism, Academic Press Inc., San Diego, CA, 1998.

[12] F. Brezzi, M. Fortin, Mixed and Hybrid Finite Element Methods, Springer-Verlag, New York, 1991.

[13] F. Cajner, B. Smoljan, D. Landek, Computer simulation of induction hardening, J. Mater. Process. Technol. 157–158 (2004) 55–60.

[14] C. Chaboudez, S. Clain, R. Glardon, D. Mari, J. Rappaz, M. Swierkosz, Numerical modeling in induction heating for axisymmetric geometries, IEEE Trans. Magn. 33 (1997) 739–745.

[15] Q.S. Chen, P. Gao, W.R. Hu, Effects of induction heating on temperature distribution and growth rate in large-size SiC growth system, J. Cryst. Growth 266 (2004) 320–326.

[16] S. Clain, J. Rappaz, M. Swierkosz, R. Touzani, Numerical modelling of induction heating for two-dimensional geometries, Math. Models Appl. Sci. 3 (1993) 805–822.

[17] G. Henneberger, R. Obrecht, Numerical calculation of the temperature distribution in the melt of industrial crucible furnaces, in: Second International Conference on Computation in Electromagnetics, April 1994.

[18] G. Henneberger, Ph.K. Sattler, D. Shen, W. Hadrys, Coupling of magnetic and fluid flow problems and its application in induction melting apparatus, IEEE Trans. Magn. 29 (1993) 1589–1594.

[19] R. Hiptmair, Symmetric coupling for eddy current problems, SIAM J. Numer. Anal. 40 (1) (2002) 41–65.

[20] R. Hiptmair, O. Sterz, Current and voltage excitation for the eddy current model, Int. J. Numer. Modelling 18 (1) (2005) 1–21.

[21] Y. Katsumura, H. Hashizume, S. Toda, Numerical Analysis of fluid flow with free surface and phase change under electromagnetic force, IEEE Trans. Magn. 32 (1996) 1002–1005.

[22] O. Klein, P. Philip, Transient numerical investigation of induction heating during sublimation growth of silicon carbide single crystals, J. Cryst. Growth 247 (2003) 219–235.

[23] B. Mohammadi, O. Pironneau, Analysis of the *k*-epsilon Turbulence Model, Wiley/Masson, New York, 1994.

[24] T.T. Natarajan, N. El-Kaddah, A methodology for two-dimensional finite element analysis of electromagnetically driven flow in induction stirring systems, IEEE Trans. Magn. 35 (3) (1999) 1773–1776.

[25] J.C. Nédélec, Acoustic and Electromagnetic Equations. Integral Representations for Harmonic Problems, Springer-Verlag, New York, 2001.

[26] O. Pironneau, On the transport–diffusion algorithm and its applications to the Navier–Stokes equations, Numer. Math. 38 (3) (1982) 309–332.

[27] J. Rappaz, M. Swierkosz, Mathematical modelling and numerical simulation of induction heating processes, Appl. Math. Comput. Sci. 6 (2) (1996) 207–221.

[28] S. Wanser, L. Krähenbühl, A. Nicolas, Computation of 3D induction hardening problems by combined finite and boundary elements methods, IEEE Trans. Magn. 30 (1994) 3320–3323.